HERMETIC PACKAGES AND FEEDTHROUGHS FOR NEURAL PROSTHESES

Quarterly Progress Report # 2

(Contract NIH-NINCDS-N01-NS-4-2319)

(Contractor: The Regents of the University of Michigan)

For the Period:

January-March 1995

Submitted to the

Neural Prosthesis Program
National Institute of Neurological Disorders and Stroke
National Institutes of Health

By the

Center For Integrated Sensors and Circuits
Department of Electrical Engineering and Computer Science
University of Michigan
Ann Arbor, Michigan 48109-2122

Program Personnel:

Professor Khalil Najafi: Principal Investigator
Graduate Student Research Assistants:
Mr. Mark Nardin: Microstimulator Circuit Design/Fabrication
Mr. Jeffrey Von Arx: Electrode and Package Fabrication/Testing
Mr. Anthony Coghlan: RF Telemetry & Microstimulator Testing
Mr. Mehmet Dokmeci: Packaging and Accelerated Testing

April 1995

SUMMARY

During the past quarter we achieved major progress in several areas, including the continued testing of our glass packages under accelerated conditions, the complete testing of the second generation microstimulator circuitry through an RF telemetry link, and continued testing of the first-generation microstimulator.

Our most significant results to date are those obtained from a series of silicon-glass packages that have been soaking in DI water at 85°C and 95°C for the past several months. We have packages that have lasted for more than 227 days at 95°C, and four that have lasted more than 221 days at 85°C in DI water. During the last quarter we lost one of the packages that was soaking at 95°C, so there are now two packages at 95°C and four at 85°C still under test without any sign of leakage in them. We had originally started with 10 samples in each category. Most of the packages that did not survive were lost primarily due to handling or due to failure within the first day. These results are impressive in that they show for the first time that these packages can survive for a long time under accelerated conditions. We also have several packages soaking at room temperature in saline for over 120 days, and these have not shown any sign of leakage either.

We explanted all four packages that were implanted in guinea pigs. These packages were placed on top of the dura, in an area where the skull had been cut away. The overall results were very promising. First, after two months of implantation there were no signs of damage to the surrounding tissue. There was no sign of infection and no adverse effects that could be detected. The implants had muscle and skull tissue completely regrown over the silicon substrate. These preliminary tests show that at least for CNS applications for a period of a few months there seems to be no problem with the packaging material. Second, we saw no damage from the biological fluids to the materials used in the package. None of the films were attacked. Third, two of the packages were still good and showed no sign of leakage after explantation. One package had fluid inside it and the other showed some leakage through electrical measurements but no visible leakage. We believe the packages that failed did so due to the mechanical forces exerted on them during implant and explant. In the coming quarter we will be processing silicon substrates with silicon ribbon cables so that we can monitor possible moisture penetration inside the package in-vivo.

We have received the new ultrasonically machined glass wafers and have diced these wafers into individual glass capsules. These capsules look very good and the overall fabrication process is very straightforward. The capsules can be bonded easily to silicon and produce very strong bonds. We have not yet performed soak tests on these capsules because the silicon substrates for their testing are not out of fabrication yet. We believe that these capsules will be easier to bond and fabricate than the previous custom-designed capsules.

During the past quarter we continued the testing of both the first-generation and the second-generation microstimulators. Two designs for the envelope detectors for the first-generation microstimulator were tested in detail and both were shown to be operational. The first-generation devices are ready for complete assembly as soon as the wafers that contain the circuit chips are completed. These wafers also include the second-generation devices. We have now completed the testing of the second-generation designs and have shown that the circuit works exactly as designed and all the blocks are fully functional. The device also has an on-chip transmitter used for establishing a bi-directional telemetry link. The transmitter uses an on-chip coil which is fabricated using electroplated nickel. The wafers are going through this fabrication step and will be ready in a few weeks. At that point, both the first-generation and the second-generation devices will be ready for assembly.

1. INTRODUCTION

This project deals with the development of hermetic, biocompatible micropackages and feedthroughs for use in a variety of implantable neural prostheses for sensory and motor handicapped individuals. The project also aims at continuing work on the development of a telemetrically powered and controlled neuromuscular microstimulator for functional electrical stimulation. The primary objectives of the project are: 1) the development and characterization of hermetic packages for miniature, silicon-based, implantable three-dimensional structures designed to interface with the nervous system for periods of up to 40 years; 2) the development of techniques for providing multiple sealed feedthroughs for the hermetic package; 3) the development of custom-designed packages and systems used in chronic stimulation or recording in the central or peripheral nervous systems in collaboration and cooperation with groups actively involved in developing such systems; and 4) establishing the functionality and biocompatibility of these custom-designed packages in *in-vivo* applications. Although the project is focused on the development of the packages and feedthroughs, it also aims at the development of inductively powered systems that can be used in many implantable recording/stimulation devices in general, and of multichannel microstimulators for functional neuromuscular stimulation in particular.

Our group here at the Center for Integrated Sensors and Circuits at the University of Michigan has been involved in the development of silicon-based multichannel recording and stimulating microprobes for use in the central and peripheral nervous systems. More specifically, during the past two contract periods dealing with the development of a single-channel inductively powered microstimulator, our research and development program has made considerable progress in a number of areas related to the above goals. A hermetic packaging technique based on electrostatic bonding of a custom-made glass capsule and a supporting silicon substrate has been developed and has been shown to be hermetic for a period of at least a few years in salt water environments. This technique allows the transfer of multiple interconnect leads between electronic circuitry and hybrid components located in the sealed interior of the capsule and electrodes located outside of the capsule. The glass capsule can be fabricated using a variety of materials and can be made to have arbitrary dimensions as small as 1.8mm in diameter. A multiple sealed feedthrough technology has been developed that allows the transfer of electrical signals through polysilicon conductor lines located on a silicon support substrate. Many feedthroughs can be fabricated in a small area. The packaging and feedthrough techniques utilize biocompatible materials and can be integrated with a variety of micromachined silicon structures.

The general requirements of the hermetic packages and feedthroughs to be developed under this project are summarized in Table 1. Under this project we will concentrate our efforts to satisfy these requirements and to achieve the goals outlined above. There are a variety of neural prostheses used in different applications, each having different requirements for the package, the feedthroughs, and the particular system application. The overall goal of the program is to develop a miniature hermetic package that can seal a variety of electronic components such as capacitors and coils, and integrated circuits and sensors (in particular electrodes) used in neural prostheses. Although the applications are different, it is possible to identify a number of common requirements in all of these applications in addition to those requirements listed in Table 1. The packaging and feedthrough technology should be capable of:

1- protecting non-planar electronic components such as capacitors and coils, which typically have large dimensions of about a few millimeters, without damaging them;
2- protecting circuit chips that are either integrated monolithically or attached in a hybrid fashion with the substrate that supports the sensors used in the implant;
3- interfacing with structures that contain either thin-film silicon microelectrodes or conventional microelectrodes that are attached to the structure;

Table 1: General Requirements for Miniature Hermetic Packages and Feedthroughs for Neural Prostheses Applications

Package Lifetime:
≥ 40 Years in Biological Environments @ 37°C

Packaging Temperature:
≤360°C

Package Volume:
10-100 cc

Package Material:
Biocompatible
Transparent to Light
Transparent to RF Signals

Package Technology:
Batch Manufactureable

Package Testability:
Capable of Remote Monitoring
In-Situ Sensors (Humidity & Others)

Feedthroughs:
At Least 12 with ≤125μm Pitch
Compatible with Integrated or Hybrid Microelectrodes
Sealed Against Leakage

Testing Protocols:
In-Vitro Under Accelerated Conditions
In-Vivo in Chronic Recording/Stimulation Applications

We have identified two general categories of packages that need to be developed for implantable neural prostheses. The first deals with those systems that contain large components like capacitors, coils, and perhaps hybrid integrated circuit chips. The second deals with those systems that contain only integrated circuit chips that are either integrated in the substrate or are attached in a hybrid fashion to the system.

Figure 1 shows our general proposed approach for the package required in the first category. This figure shows top and cross-sectional views of our proposed approach here. The package is a glass capsule that is electrostatically sealed to a support silicon substrate. Inside the glass capsule are housed all of the necessary components for the system. The electronic circuitry needed for any analog or digital circuit functions is either fabricated on a separate circuit chip that is hybrid mounted on the silicon substrate and electrically connected to the silicon substrate, or integrated monolithically in the support silicon substrate itself. The attachment of the hybrid IC chip to the silicon substrate can be performed using a number of different technologies such as simple wire bonding between pads located on each substrate, or using more sophisticated techniques such as flip-chip solder reflow or tab bonding. The larger capacitor or microcoil components are mounted on either the substrate or the IC chip using appropriate epoxies or solders. This completes the assembly of the electronic components of the system and it should be possible to test the system electronically at this point before the package is completed. After testing, the system is packaged by placing the glass capsule over the entire system and bonding it to the silicon substrate using an electrostatic sealing process. The cavity inside the glass package is now hermetically sealed against the outside environment. Feedthroughs to the outside world are provided using the grid-feedthrough technique discussed in previous reports. These feedthroughs transfer the electrical signals between the electronics inside the package and various elements outside of the package. If the package has to interface with conventional microelectrodes, these microelectrodes can be attached to bonding pads located outside of the package; the bond junctions will have to be protected from the external environment using various polymeric encapsulants. If the package has to interface with on-chip electrodes, it can do so by integrating the electrode on the silicon support substrate. Interconnection is simply achieved using on-chip polysilicon conductors that make the feedthroughs themselves. If the package has to interface with remotely located recording or stimulating electrodes that are attached to the package using a silicon ribbon cable, it can do so by integrating the cable and the electrodes again with the silicon support substrate that houses the package and the electronic components within it.

Figure 2 shows our proposed approach to package development for the second category of applications. In these applications, there are no large components such as capacitors and coils. The only component that needs to be hermetically protected is the electronic circuitry. This circuitry is either monolithically fabricated in the silicon substrate that supports the electrodes (similar to the active multichannel probes being developed by the Michigan group), or is hybrid attached to the silicon substrate that supports the electrodes (like the passive probes being developed by the Michigan group). In both of these cases the package is again another glass capsule that is electrostatically sealed to the silicon substrate. Notice that in this case, the glass package need not be a high profile capsule, but rather it need only have a cavity that is deep enough to allow for the silicon chip to reside within it. Note that although the silicon IC chip is originally 500μm thick, it can be thinned down to about 100μm, or can be recessed in a cavity created in the silicon substrate itself. In either case, the recess in the glass is less than 100μm deep (as opposed to several millimeters for the glass capsule). Such a glass package can be easily fabricated in a batch process from a larger glass wafer.

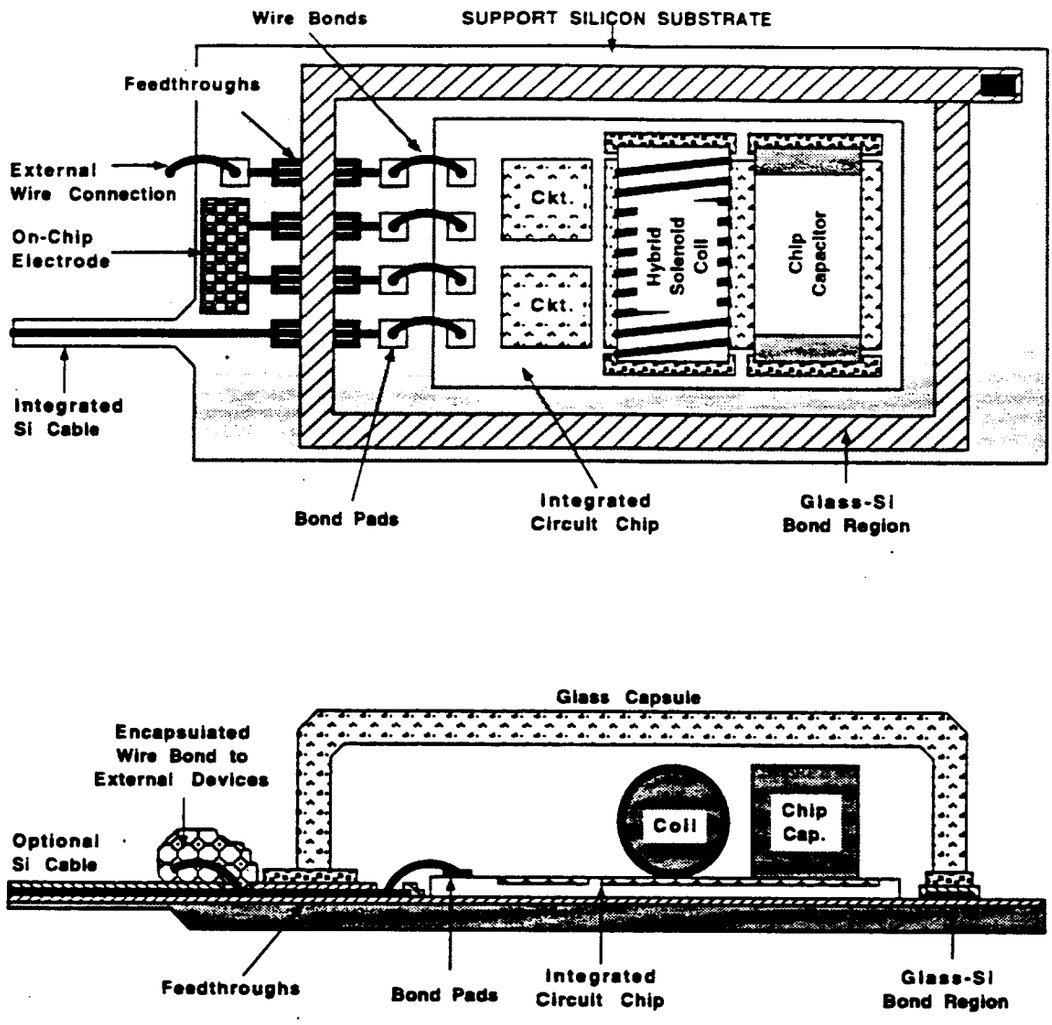

Figure 1: A generic approach for packaging implantable neural prostheses that contain a variety of components such as chip capacitors, microcoils, and integrated circuit chips. This packaging approach allows for connecting to a variety of electrodes.

We believe the above two approaches address the needs for most implantable neural prostheses. Note that both of these techniques utilize a silicon substrate as the supporting base, and are not directly applicable to structures that use other materials such as ceramics or metals. Although this may seem a limitation at first, we believe that the use of silicon is, in fact, an advantage because it provides several benefits. First, it is biocompatible and has been used extensively in biological applications. Second, there is a great deal of effort in the IC industry in the development of multi-chip modules (MCMs), and many of these efforts use silicon supports because of the ability to form high density interconnections on silicon using standard IC fabrication techniques. Third, many present and future implantable probes are based on silicon micromachining technology; the use of our proposed packaging technology is inherently compatible with most of these probes, which simplifies the overall structure and reduces its size.

Once the above packages are developed, we will test them in biological environments by designing packages for specific applications. One of these applications is in recording neural activity from cortex using silicon microprobes developed by the Michigan group under separate contracts. The other involves the chronic stimulation of muscular tissue using a multichannel microstimulator for the stimulation of the paralyzed larynx. This application has been developed at Vanderbilt University. Once the device is built, it will be used by our colleagues at Vanderbilt to perform both biocompatibility tests and functional tests to determine package integrity and suitability and device functionality for the reanimation of the paralyzed larynx. The details of this application will be discussed in future progress reports.

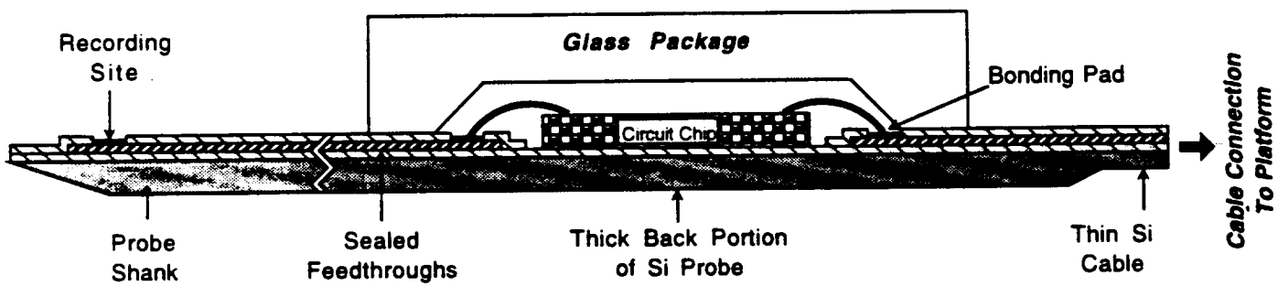

Figure 2: Proposed packaging approach for implantable neural prostheses that contain electronic circuitry, either monolithically fabricated in the probe substrate or hybrid attached to the silicon substrate containing microelectrodes.

2. ACTIVITIES DURING THE PAST QUARTER

2.1 Hermetic Packaging

Over the past few years we have developed a bio-compatible hermetic package with high density, multiple feedthroughs. This technology utilizes electrostatic bonding of a custom-made glass capsule to a silicon substrate to form a hermetically sealed cavity, as shown in Figure 3. Feedthrough lines are obtained by forming closely spaced polysilicon lines and planarizing them with LTO and PSG. The PSG is reflowed at 1100°C for 2 hours to form a planarized surface. A passivation layer of oxide/nitride/oxide is then deposited on top to prevent direct exposure of PSG to moisture. A layer of fine-grain polysilicon (surface roughness <40Å rms) is deposited and doped to act as the bonding surface. Finally, a glass capsule is bonded to this top polysilicon layer by applying a voltage of 2000V between the two for 10 minutes at 320°C, a temperature compatible with most hybrid components. The glass capsule can be either custom molded from Corning code #7740 glass, or can be batch fabricated using ultrasonic micromachining of #7740 glass wafers.

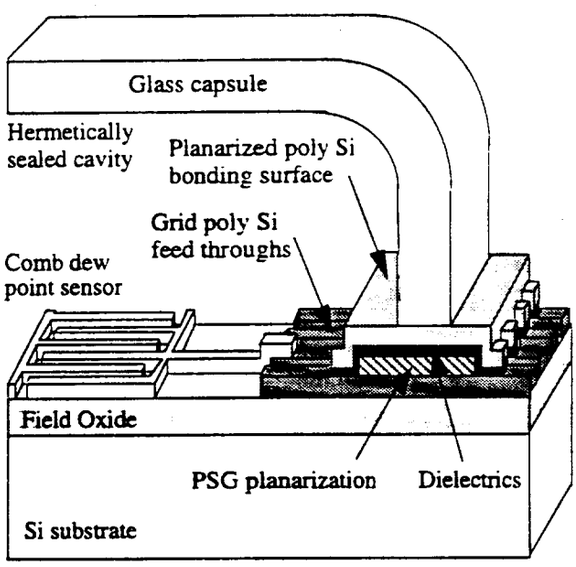

Figure 3: The structure of the hermetic package with grid feedthroughs.

During the past year we have electrostatically bonded and soak tested close to one hundred of these packages. We have found that the strongest and most reproducible bonds are obtained when we follow the bonding procedure outlined in Table 2. Subsequently, all of the packages used in the soak tests and the in vivo tests reported here have been bonded with this technique. Our bonding yield using this technique is now 85% (yield is defined as the percentage of packages which last more than 24 hours soaking in DI water), and with this technique the packages successfully prevent leakage in soak tests at 95°C for over 3 months on average.

2.1.1 Accelerated Soak Tests

We have continued accelerated soak testing of the packages that have been under test. For these tests we have chosen temperature as the acceleration factor because it is an easy

variable to control, and because moisture diffusion is a strong (exponential) function of temperature. We started soaking 10 samples each at 95°C and 85°C in this series of tests. Tables 3 and 4 list some pertinent data for these soak tests. Figure 4 summarizes the results so far from the 95°C soak tests and Figure 5 summarizes the results so far from the 85°C tests. These figures also list the causes of failure for individual packages when it is known, and they show a curve fit to our lifetime data to illustrate the general trend. The curve fit, however, only approximates the actual package lifetimes since many of the packages failed due to breaking and excessive handling during testing rather than due to leakage.

Table 2: Table outlining the bonding technique that consistently gives us high quality bonds.

Step	Comments
Packaging wafer is thinned and separated into individual packaging substrates	Best results are obtained when the package is thinned to between 100-150 μm (Our new ultrasonically machined glass capsules should eliminate the need to thin the silicon wafer.)
Packaging substrates with obvious defects are discarded	All packaging substrates are visually inspected before bonding and those with either obvious lithography defects or scratches anywhere on the bonding region are discarded. About 30% of our packaging substrates are discarded in this way.
Capsule and substrate are solvent cleaned	Our clean consists of TCE, then acetone, then IPA and finally DI water, all hot and with ultrasound agitation
Conductive coating is sputtered on glass capsule	Either sputtered aluminum or silver epoxy works well
Electrostatic bonding	Substrate is first placed on 320 to 340°C hot plate and glass capsule is aligned. A Pyrex cover is then placed over sample. Probes are lowered through hole in the Pyrex to make electrical contact. 2000V is applied for 10 minutes. Structure is cooled slowly (≈20 minutes to cool to RT)
Conductive coating removed	Aluminum enchant does this quickly

Table 3: Key data for 95°C soak tests in DI water.

Number of packages in this study	10
Failed within 24 hours (number discarded)	1
Packages lost due to mishandling	2
Longest lasting packages so far in this study	227 days
Packages still under tests with no measurable room temperature condensation inside	2
Average lifetime to date (MTTF)	*90 days*

Table 4: Key data for 85°C soak tests in DI water.

Number of packages in this study	10
Failed within 24 hours (number discarded)	2
Packages lost due to mishandling	3
Longest lasting packages so far in this study	221 days
Packages still under tests with no measurable room temperature condensation inside	4
Average lifetime to date (MTTF)	*116 days*

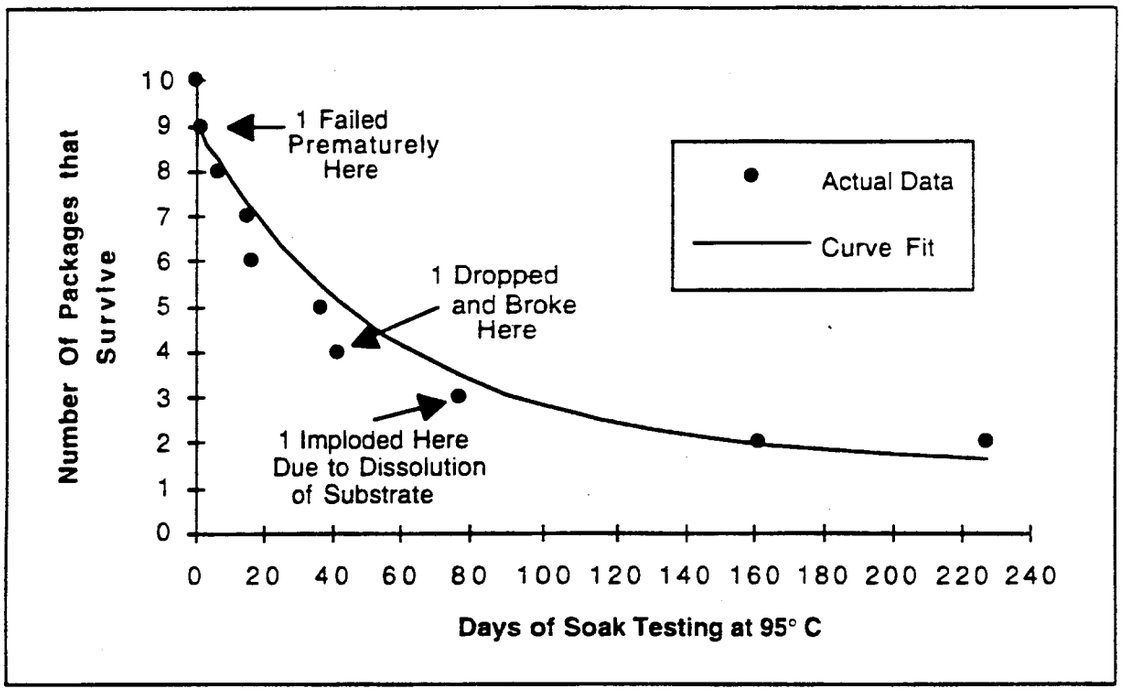

Figure 4: Summary of the lifetimes of the 10 packages which have been soak tested at 95°C.

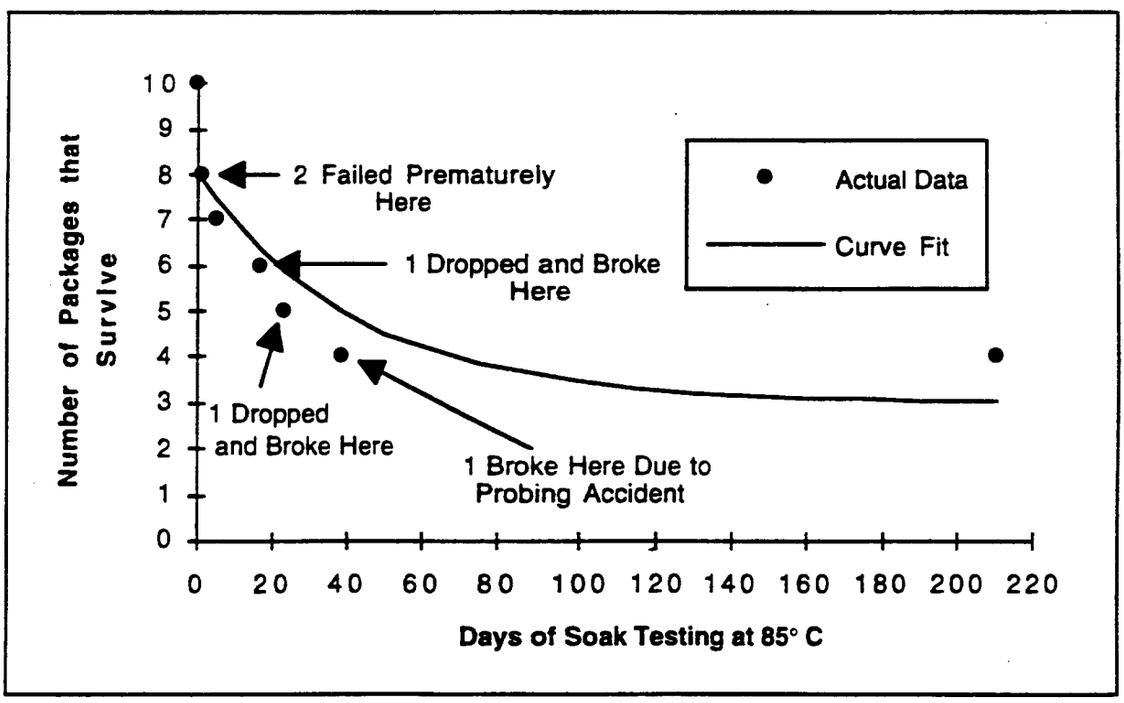

Figure 5: Summary of the lifetimes of the 10 packages which have been soak tested at 85°C.

During the last quarter one more of the packages that was soaking at 95°C failed, leaving only two soaking at this temperature. Therefore, the longest lasting packages at this temperature have survived for more than 227 days. There are four packages left at 85°C with the longest one having survived for 221 days. Tables 3 and 4 also show the MTTF for the packages at the two different temperatures. If we use an activation energy of about Q=-0.946eV, we get an MTTF of more than fifty years at body temperature. Until we determine the activation energy more accurately we will not be able to provide an accurate MTTF at body temperature. Of course, we will try to do this during the next few years. We will continue the 85°C and 95°C accelerated soak tests in the coming quarter. We hope to add many more packages to these tests, including at least 10 made using the new ultrasonically machined glass capsules. Also, we hope to begin saline soak tests at these accelerated temperatures to more closely mimic biological conditions.

2.1.2 Room Temperature Soak Tests

We began some long term soak tests in phosphate buffered saline at room temperature last quarter. We started these tests for two reasons. First, we want tests in saline, and so far we have only been able to perform accelerated tests in DI water due to the dissolution of silicon in saline at high temperature. Secondly, it is useful to obtain some soak test data without any acceleration just to see if any gross failures occur. These room temperature tests could go for a long time and we intend to let them continue as long as we can. The results obtained this way will act as a good control technique to verify the overall integrity of the package. It should be noted that we are also setting up to perform tests at 37°C to mimic the body environment.

We have 6 packages soaking in saline at room temperature. One of these packages leaked within a day, indicating surface defects or poor alignment of the glass capsule to the silicon substrate. Note that in the last quarter report we erroneously reported that 2 of these 6 packages leaked within a day. What we thought was leakage that we could visually see in one of these packages turned out not to be. We routinely assume that anything that looks like it might possible be moisture, is moisture until we can prove otherwise. With this particular package, continued observation and dozens of electrical measurements on our dew point sensors showed that there was in fact no moisture inside. All five packages that are all still soaking show no sign of moisture either measured electrically or observed visually. Three of these five packages have been soaking now for 120 days, one for 86 days, and the fifth package has been soaking for 79 days. Table 5 summarizes the results from room temperature soak tests.

Table 5: Data for room temperature saline soak tests in saline.

Number of packages in this study	6
Failed within 24 hours (number discarded)	1
Longest lasting packages so far in this study	120 days
Packages still under tests with no measurable room temperature condensation inside	5
Average lifetime to date (MTTF)	*105 days*

2.1.3 In-Vivo Tests

Last quarter we began in-vivo testing of the hermetic package. Four devices were implanted in three guinea pigs at Kresge Hearing Research Institute. These devices were placed on top of the dura, in an area where the skull had been cut away. The skin was then sutured together, leaving the devices sitting on top of the dura, not fixed in place. This placement is

compatible with the eventual placement of the hermetically-packaged telemetry platforms for application in the CNS. This quarter all four of these implanted devices were explanted after 2 months in-vivo. Table 6 summarizes details for each of these in-vivo tests.

After 2 months in-vivo, only one of these packages had gross leakage, one had a slight amount of leakage that we could only detect electrically, and the final two packages had no observable moisture inside, although the substrates broke during explant, so we could not probe these last two devices electrically. We should mention that all of these devices were soaked in DI water at 95°C for a number of days before implanting to make sure that there were no imperfections in the bonding surfaces or misalignment of the glass capsule that might lead to a quick failure of the package. Because of this, we do not believe that failure in the two devices that leaked was due to defects. Rather, we believe that it was probably due to excessive mechanical forces that may have damaged the package. In both of these implants we noticed that skin had grown up around them rather than over them, as shown in Figure 6. The skin fixed itself around the glass capsule in these two animals, and healthy skull and muscle tissue grew up around the silicon substrate, fixing the substrate firmly to the skull. Thus any movement of the animals skin put strain directly on the glass-silicon anodic bond, eventually breaking the one package that had gross amount of fluid inside of it, and probably weakening the other package that had trace amounts of moisture. More care can be taken during implant to avoid this. This problem did not happen in animal implants #1 and #2 in Table 6, which were both in the same animal. The glass capsule of these packages did not poke up through the skin because one central incision was made and the two devices were implanted to the left and right of the incision, rather than directly under the incision. Because the devices were not right under the incision, the glass capsule did not get in the way of the regrowing skin.

After two months in-vivo, all of the implants had healthy tissue growing up around the implants. There was no sign of infection in any of the implanted animals, and no adverse effects that our histology technician could determine. The first two implants had muscle completely regrown over the entire package, and the skull had over grown the substrate and was beginning to encapsulate the glass. The second two implants had muscle and skull tissue completely regrown over the silicon substrate, but as already mentioned, the top of the glass capsule was sticking through the skin. Figure 7 shows one of these latter two devices during explant before most of the encapsulating skull and muscle tissue had been removed. Figure 8 shows another of these devices on explant after the skull and muscle tissue has been carefully cut away down to the silicon substrate. We do not believe that migration of these devices will be a problem for CNS applications because the skull and muscle tissue that grew up around all of the implanted devices securely fixed them in place. In fact, this is what made the devices difficult to remove, and led to the breakage of 3 of them during explant.

Examination of the silicon substrate from all four explanted devices showed no indication of dissolution of the silicon substrate or the polysilicon films. There was no sign of etching of any of the thin films used in the packaging process. Figure 9 shows a photograph of one of the substrates after explant and after the glass capsule has been removed. All of the patterned layers can be clearly seen in the photograph to have no damage, and the substrate contains no etch pits. We should mention that we did not expect any damage to any of the layers used in the package or to the substrate itself at body temperature, but as mentioned in our previous reports, we have observed damage in our accelerated soak tests in saline at high temperatures.

We believe that these preliminary in-vivo results show that this package is bio-compatible and rugged. Healthy tissue had grown up around all of the implanted packages, and we observed no dissolution of the silicon substrate. Unfortunately, most of these packages broke during explant, so we were only able to obtain electrical leakage measurements on one of them, but visual inspection before the packages broke showed that there was not gross leakage on three out of four of the packages. In our next design iteration, we plan on adding ribbon cable leads to

the packaging substrate for in-situ monitoring of the dewpoint sensors inside of the package. Also, we have a new substrate which we are currently fabricating that has much smaller silicon substrate area sticking out from the glass capsule, which we believe will be much less prone to breakage. Finally, we hope that the new ultrasonically machined glass capsules will allow us to not have to thin the silicon substrate to 100-150μm before bonding. Packages made with silicon substrates that are the full 500μm thick should be much less prone to breakage.

Table 6: Summary of the in-vivo tests concluded this quarter.

Implant Number	Guinea Pig Number	Date of Implant	Number of days Implanted	Gross Leakage Visually Observed During Explant	Device Broke During Explant	Comments
Implant #1	GP #1	Jan 17, 1995	62 days	No	Yes	Visual inspection in-situ showed no sign of leakage.
Implant #2	GP #1	Jan 17, 1995	62 days	No	Yes	Visual inspection in-situ showed no sign of leakage.
Implant #3	GP #2	Feb 2, 1995	61 days	Yes	Yes	Visual inspection in-situ showed that this device had obvious gross leakage. Skin had grown up around implant, no over it.
Implant #4	GP #3	Feb 17, 1995	61 days	No	No	Only package explanted without damage. Although visual inspection indicated no gross leakage, electrical measurements showed that the package had leaked. Skin had also grown up around this implant, not over it, which may have contributed to the leakage.

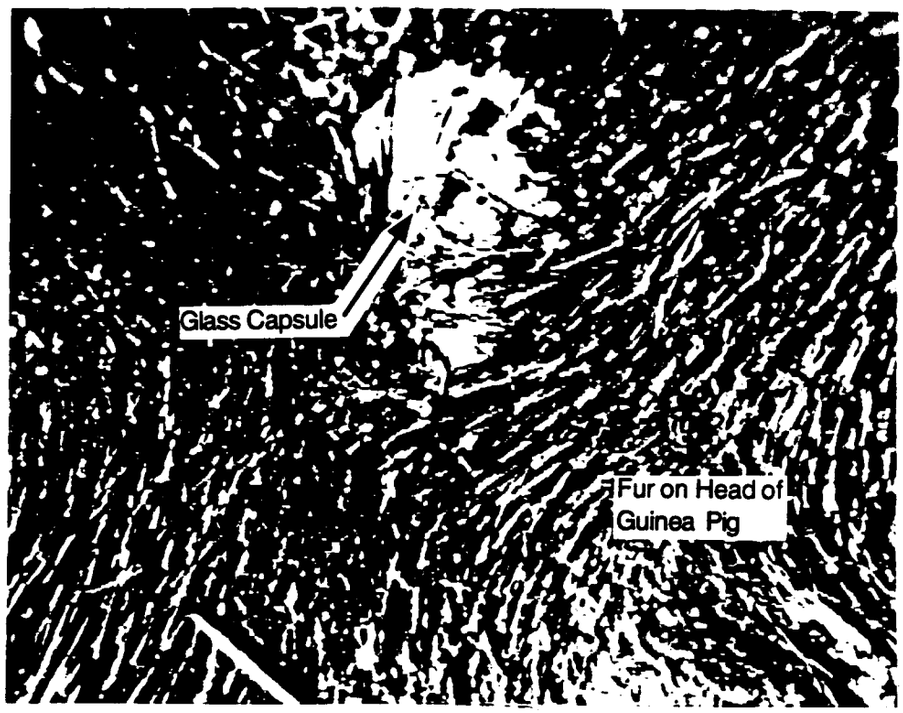

Figure 6: A photograph of the skin of animal GP#4 taken two months after a packaged device was implanted in it. The skin has grown up around the glass capsule, but not over it. The glass capsule is clearly visible in the center of the photograph.

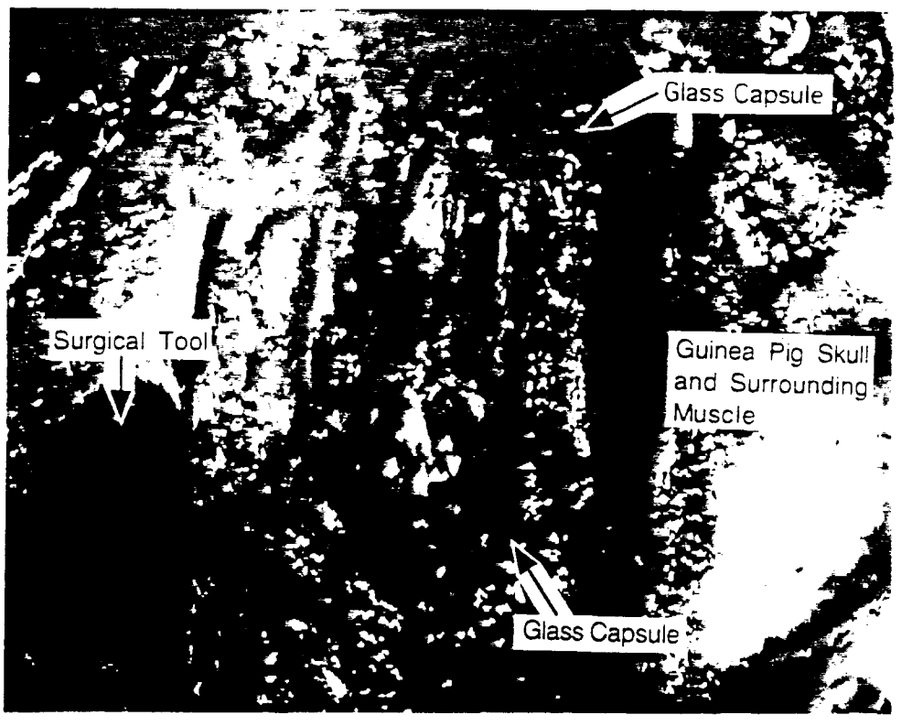

Figure 7: A photograph of one of the devices after being implanted for 2 months. The muscle and skull have completely re-grown over the entire silicon substrate.

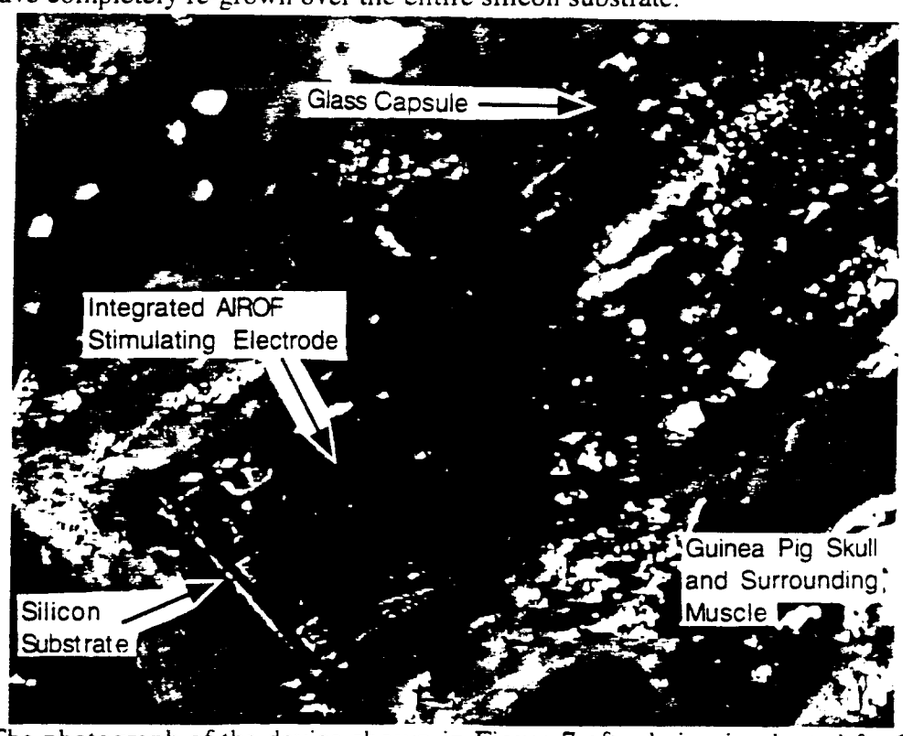

Figure 8: The photograph of the device shown in Figure 7 after being implanted for 2 months. The muscle and skull tissue have been cut away to reveal the silicon substrate and the stimulating electrode.

Figure 9: A photograph of the substrate from a package that was explanted after two months in-vivo. The glass capsule was deliberately broken off for this picture. The area of the substrate that was inside of the package is free of stains left by bodily fluids. This substrate broke during explant, and the broken end can be seen on the right in this photograph. There is no apparent dissolution of any of the films in this photograph.

2.1.4 New Glass Capsules

As mentioned in the past reports, the ultrasonically machined glass capsules have several advantages over the previous custom made glass capsules, including lower cost, batch fabrication, and better surface polish over the bonding areas. During the past quarter, we received 10 glass wafers each containing about 80 ultrasonically machined glass substrates with 2 different designs. After obtaining these wafers during this quarter, we have begun preliminary dicing and bonding experiments with these new glass packages. Figure 10 below shows a SEM picture of one of these new glass packages after it is diced and cleaned.

The main feature of these new packages is that they have been individually machined on a 4" glass wafer and they can be diced with an in-house dicing machine. Our preliminary experiments show that these glass wafers can be diced to produce very small sidewall thickness. We have been dicing these glass capsules with a thickness of about 300μm with no difficulties. One of the main issues during the dicing procedure was the damage done both on the bonding surface and the sidewalls of the glass capsule. We have observed little chipping due to dicing, but as seen in the SEM view in Figure 11 the size of the chips is not significant compared to the size of the entire bonding region. Typically the chipping dimensions are about 20μm and which will not effect the hermeticity of our bonds. It is also observed that after dicing, the surfaces look smooth and uniform with no sharp extensions. The sidewall of the glass package after dicing is not very smooth, as can be seen in Figure 12. These sidewalls can be perhaps polished slightly by etching in BHF. This experiment has not been performed yet, but is planned for the coming quarter.

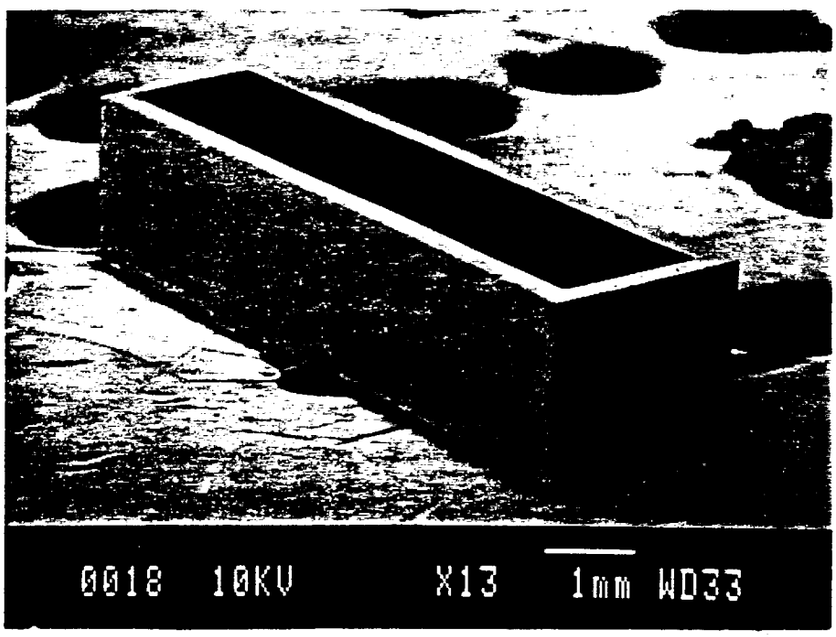

Figure 10: A SEM photograph of a new, ultrasonically machined glass capsule after it is diced and cleaned.

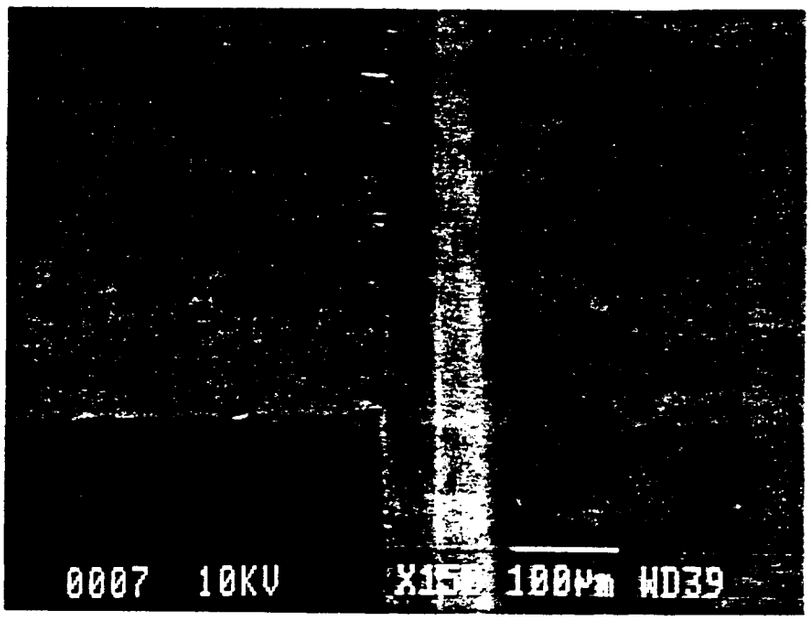

Figure 11: SEM photograph showing a close-up view of the corner of one of the diced capsules. Note that the worst chipping is still much smaller than the thickness of the capsule wall.

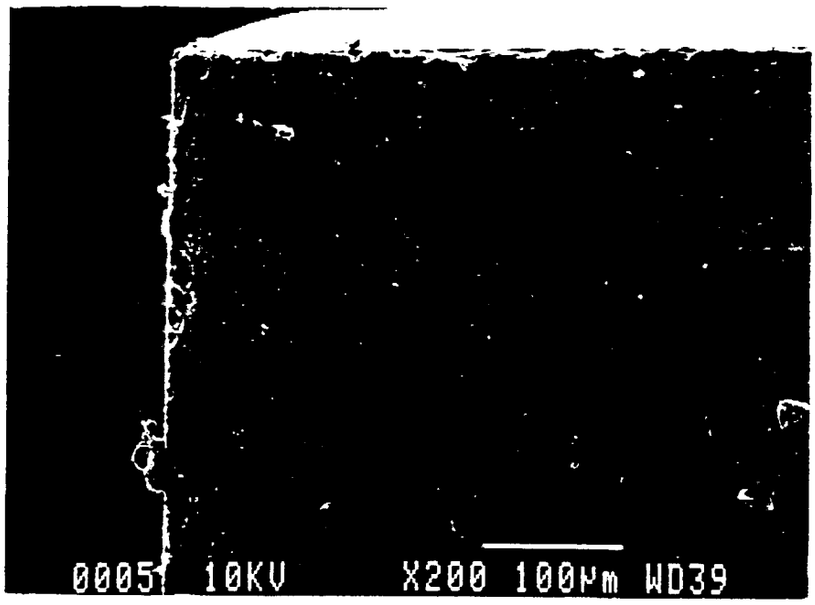

Figure 12: SEM photograph of the glass capsule sidewall after it has been diced.

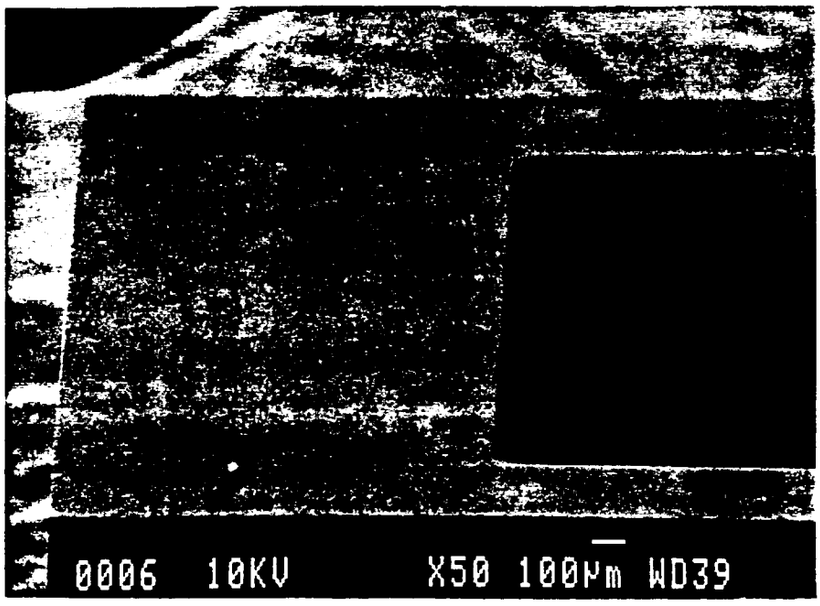

Figure 13: Close-up SEM photograph of the bonding surface of one of the glass packages. It can be seen that the bonding surface is very smooth.

It is most probable that these diced surfaces of the new glass packages will not cause problems for the in-vivo implantation studies in the future. Moreover, the bonding surface of these new glass packages after they have been diced have been inspected. Figure 13 shows a typical bonding surface of a glass package. In order to have a better view of the bonding surface this one has been diced much wider in one dimension than the others. The bonding surface seems smooth. Experiments with bonding these glass substrates to bare silicon have been performed, as discussed in the next section.

2.1.5 Bonding Experiments With The New Glass Packages

After having obtained a smooth bonding surface we have done preliminary bonding experiments with these new substrates to bare silicon wafers. During the time of these experiments the packaging substrates were still being processed and as such, data regarding these bonding experiments with the silicon package substrates will be reported during the coming quarter. Our initial experiments verify that we can bond the new glass substrates to bare silicon at 320°C with our previous bonding procedure (using 2000V for 10 minutes). Several bonds made at this temperature have been manually pulled apart and show the existence of a strong anodic bond between the silicon and the glass. All the bonds at this temperature have very thick glass remnants left all over the bonding region and convey the fact that the bond is a very strong bond. Moreover, with the desire to reduce our bonding temperature we have done experiments at lower temperatures down to 300°C. Figure 14 shows an SEM photograph of the bonding region after the glass package is pulled apart from the silicon substrate. This bond which was made at 300°C for 10 minutes is an excellent bond, illustrating the fact that it is stronger than both the glass and the silicon.

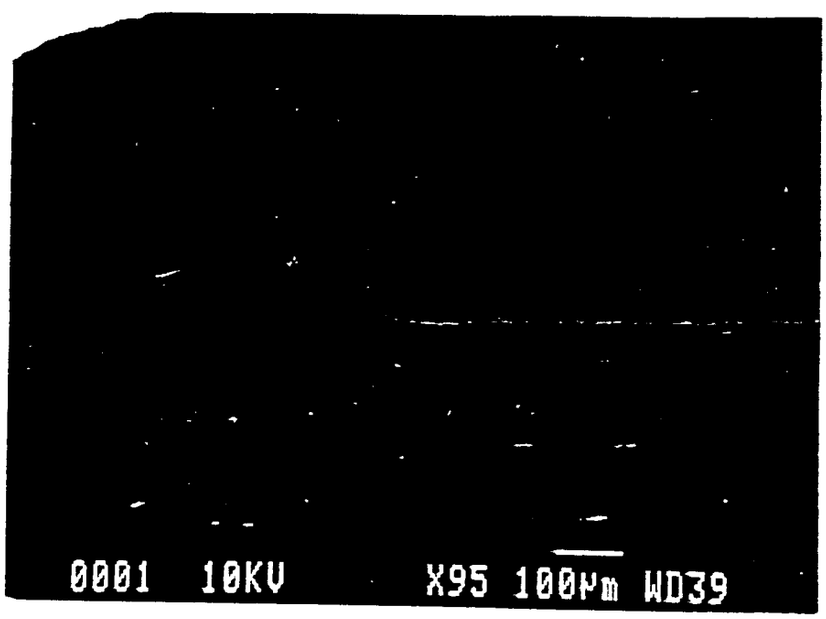

Figure 14: SEM photograph of a bonding region after the glass package is pulled apart from the silicon substrate. The bond was performed at 300°C for 10 minutes.

The fact that we have been able to obtain very strong bonds from our experiments suggest that we may be able to eliminate the thinning step before bonding which in turn would increase the mechanical strength of our packages. We intend to do more lower temperature bonding experiments at different times and different temperatures using silicon and fine-grain polysilicon in the coming quarter. We are also planning to determine the hermeticity of these packages by actually soaking them in deionized water at higher temperatures. These tests will begin as soon as we have finished the fabrication of the new silicon package substrates. The results obtained from the ultrasonically machined capsules are very encouraging and indicate that several of the potential problems with regard to the glass capsule may be resolved. We hope to be able to obtain results in all of these areas during the coming months.

2.1.6 Effect Of High Temperature Heat Cycling Of Microcoils

In order to better understand some of the potential problems that may arise in the packaging of the complete microstimulator, we performed studies of how the microcoils' electrical and physical properties might change from cycling at the temperature used for our anodic bonding, ≤340°C. The results gave us useful information on some precautions that we may have to take to ensure the success of the complete system.

The tests were performed on four very similar microcoils. All of them consisted of 90 to 100 turns wound around cores of the size that we intend to use inside the glass package, i.e. 3.5mm (len.) x 1.0mm (diam.). After winding, the coils were coated with polyimide and baked at 180°C for about 20 minutes, principally to set the windings in place. Then the leads were stripped with a commercially available chemical wire enamel stripper. The coils were subsequently measured on a carefully compensated gain-phase analyzer at 2.00 MHz. Following this initial preparation, the microcoils were heated on a silicon wafer placed on a hotplate at 340°C for 10 minutes, removed, and cooled by placing the wafer on a glass slide.

After this initial heat cycling, the coils were measured again, their leads having been gently cleaned by passing them between the tips of metal tweezers. The coils' inductance, series resistance, and Q values were compared to the initial measured values. It was observed that the series resistance and inductance increased very slightly but that the resistance increased proportionally more than the inductance. Consequently the Q values decreased slightly. Nonetheless, the variation from the initial values was essentially insignificant. The principal change observed was a considerable darkening in physical appearance of the coils, indicating that the polyimide and underlying enamel were very possibly further curing from the heat cycling and thus potentially outgassing. This condition would be almost certainly detrimental to the quality of the package sealing process. The development suggested that we should further cycle the microcoils at 340°C for a sufficient amount of time, until the coils did not seem to be changing anymore plus several minutes for a safety margin.

Thus we repeated the heat cycling process for an additional half hour. All procedural conditions were maintained as identical as possible to those in the first cycle. The microcoils were again removed, cooled, and measured on a gain-phase analyzer. Again, the electrical properties remained virtually the same as initially measured. This time we were careful to clean the coil leads as described previously, but more thoroughly. It was found that the slight increase in resistance that we had come to expect actually decreased by this gentle but thorough treatment. Clearly this was an indication that the very thin layer of surface oxide forming on the bare leads from heating the coils was probably the dominant mechanism behind this increase in series resistance. It is very necessary to be gentle in this cleaning since all additional handling of the leads increases the probability that they may become too fragile to be bonded to a microstimulator's pads.

The data from these measurements are presented in Figures 15 to 17. Clearly, the variation in electrical properties cannot be considered to indicate any particular trend from heat cycling and is essentially insignificant. The electrical properties remain basically unchanged. This was an important observation, since it indicates that the high temperature alone will not damage the coils in any way that may affect our ability to accurately predict and define the microstimulator's tuned frequency. It remains to be seen that sparking within the capsule will not occur and damage the coil when the full assembly is performed. These are tests that we will do very soon. Furthermore, the tests actually suggested that extended heat cycling is a necessary step in preparation of the microcoils for incorporation into the entire package.

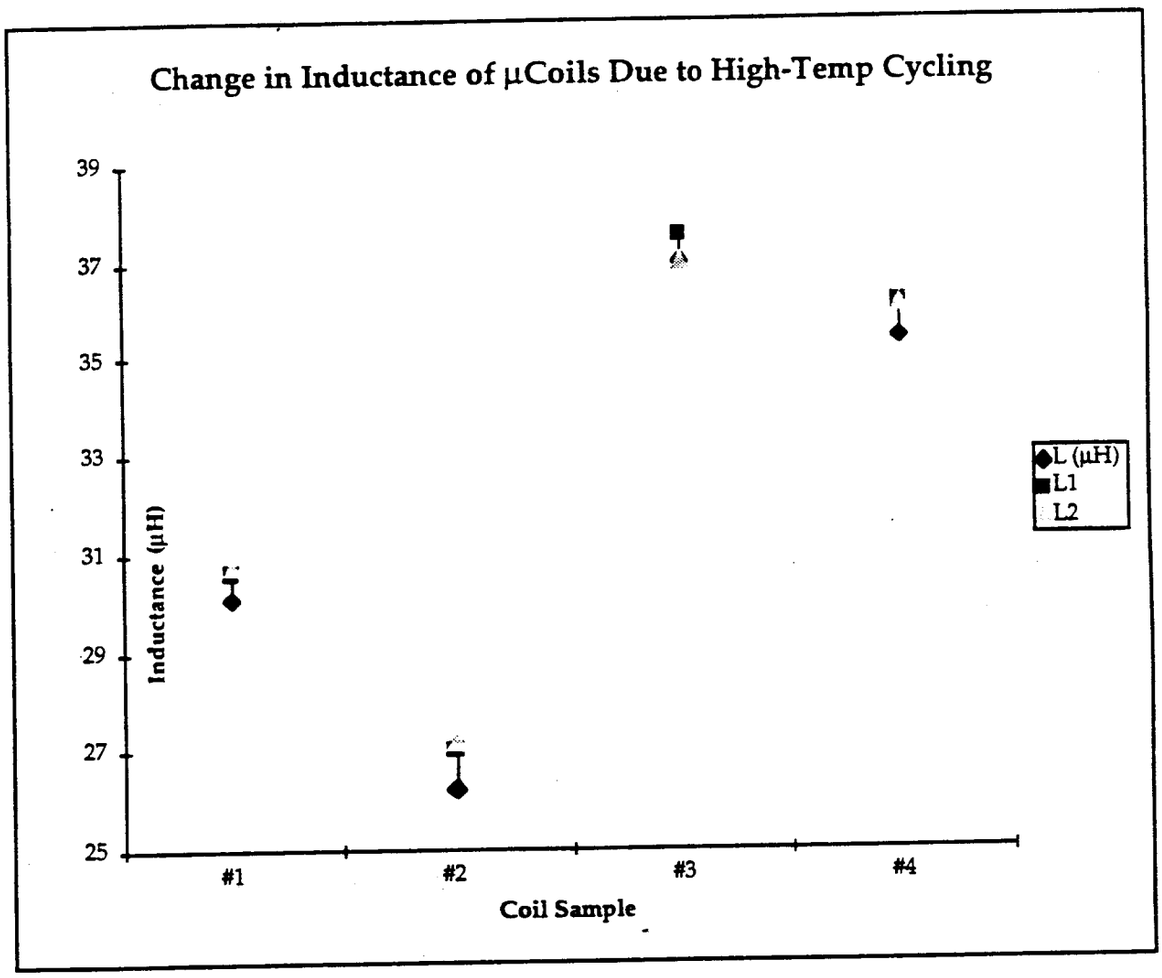

Figure 15: The effect of subjecting the microcoils to 340°C for an extended time is shown here. "L" is the reference set. "L1" indicates the results after 10 minutes (first cycle) and "L2" illustrates the results after an additional 30 minute cycle.

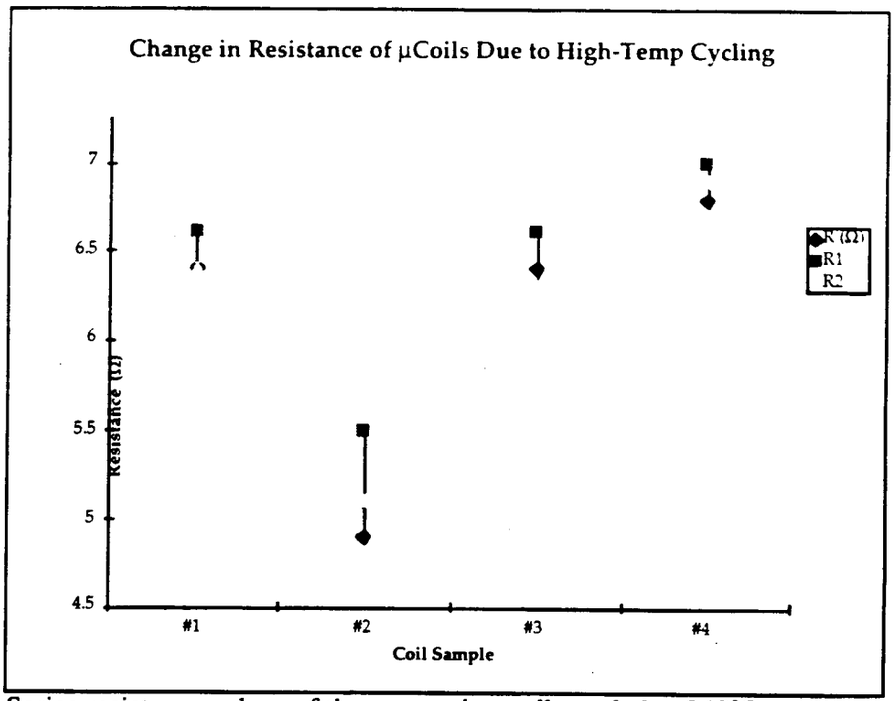

Figure 16: Series resistance values of the same microcoils cycled at 340°C are illustrated. "R" is the reference set. "R1" indicates the results after 10 minutes (first cycle) and "R2" shows the results after a further 30 minute cycle.

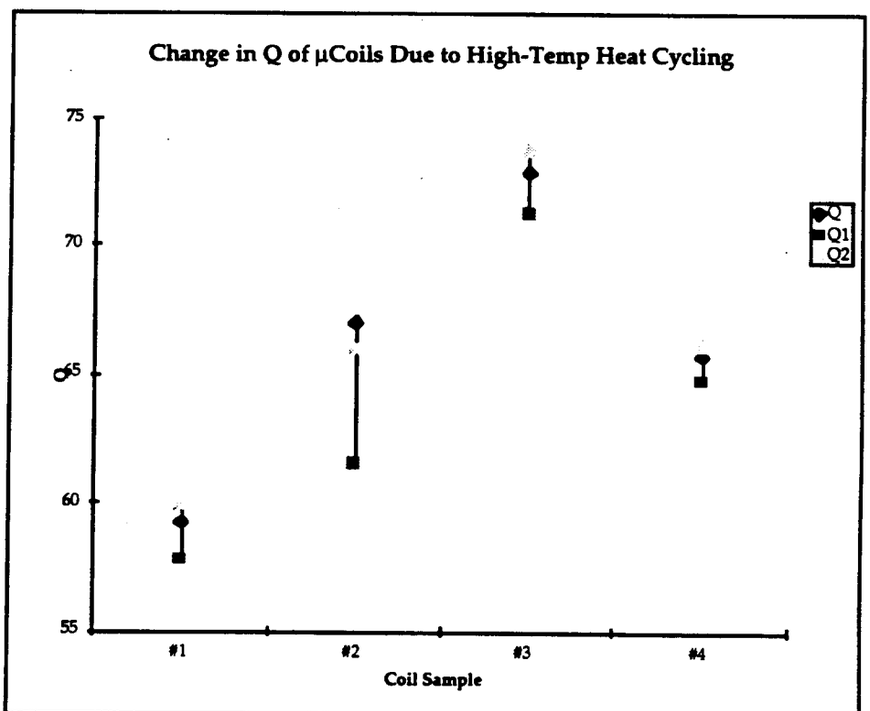

Figure 17: The Q values of the same coils cycled at 340°C are shown here. "Q" is the reference set. "Q1" values were measured after the first cycle (10 minutes) and "Q2" were measured after an additional 30 minutes.

2.1.7 Microwelding Of Coils To Microstimulator Chips

To bond the microcoils onto the microstimulators, we intend to utilize a technique called microwelding, in which two precisely controlled electrodes separated by a very small gap are brought down upon the wire to be bonded, pinning it to the bonding pad and welding it there as a high current pulse is released into the wire held between the electrodes. Here we present initial results on our use of this technique, as we have just begun to utilize it effectively.

We found that there were several factors affecting the quality of our microwelded bonds initially. The principal factor was the surface preparation of the wire and bonding pads. Any significant debris or film, including remnants of the wire's enamel, could easily increase the access resistance to these surfaces to the point that the microwelder's current decreased immensely and failed to produce a bond. Cleaning of the pads with an acetone, alcohol, deionized water sequence has so far proven adequate. We have found that the wire welds best when prepared by first flattening the ends slightly and then carefully stripping mechanically. To strip chemically so close to the coil windings would be precarious. Another critical factor was that the first layer aluminum of the microstimulator chips was too thin to tolerate the microwelding. Actually, an occasional bond would result well, but far too many tended to be weak if the welding parameters were eased or otherwise destructive to the pad if the parameters were increased to try to get a stronger bond. The pad would often melt and draw in upon itself.

Suspecting that a bond would work much better to a thicker metal layer, we tried microwelding to nickel electroplated structures. These tests so far have been very successful. Figure 18 illustrates such a microwelded bond. We have been able to bond wire prepared as indicated above to nickel pads as small as about 50µm x 50µm. The bonds appear to be strong, with neither the wire nor the pads damaged. These tests are quite recent, so we have not been able to confirm electrical continuity at the weld site. Nonetheless, visual inspection shows what appears to be a well fused union. Furthermore, as indicated previously, the slightest debris or surface pollutants act to prevent a bond, so it is suspected that the two metals have indeed come into contact and melted together effectively in what should be a low resistance weld. We are currently in the process of nickel electroplating a second metal layer on our microstimulator chips, and it is to this thicker layer that we will microweld the inductor coils as well as attach the charge storage capacitors. Considering the initial success of the microwelding technique with copper wire and nickel electroplated structures, we are fairly confident that we shall be able to attach the microcoils to their bonding pads without considerable difficulty.

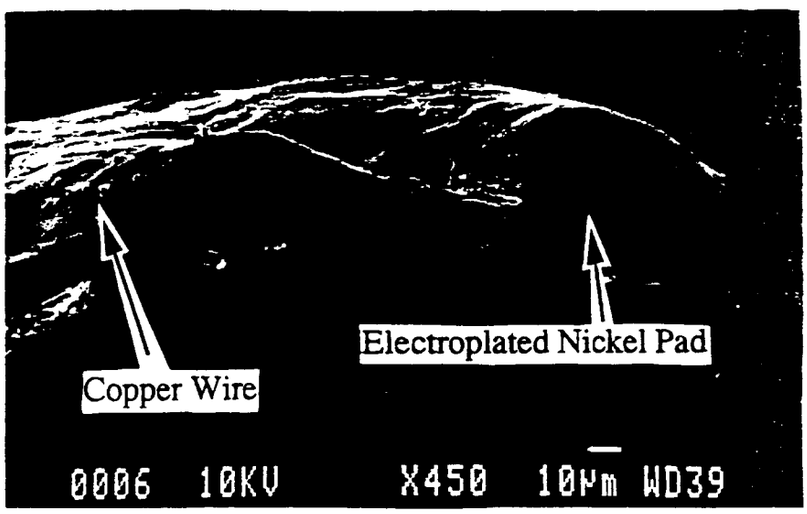

Figure 18: SEM image of a copper wire microwelded to a nickel electroplated pad.

2.2 Implantable Microstimulators

2.2.1 Single-Channel Microstimulator

Figure 19 shows the overall circuit block diagram for the single-channel microstimulator. In the last quarterly report we provided details on the functioning of all of the circuit blocks of this device. The results were quite good for every block except for the envelope detector. During this quarter we worked on more complete characterization of the envelope detection circuitry, and the results of this testing are presented below.

Envelope Detector Test Results

In previous microstimulator circuit fabrication runs, one of the circuit blocks that has proven to be the least reliable has been the envelope detection circuitry. For this reason, in the latest circuit design there were two versions of envelope detection circuitry included on chip. The two different circuits are shown in Figure 20 and Figure 21. The method of operation of each of these circuit blocks is described below.

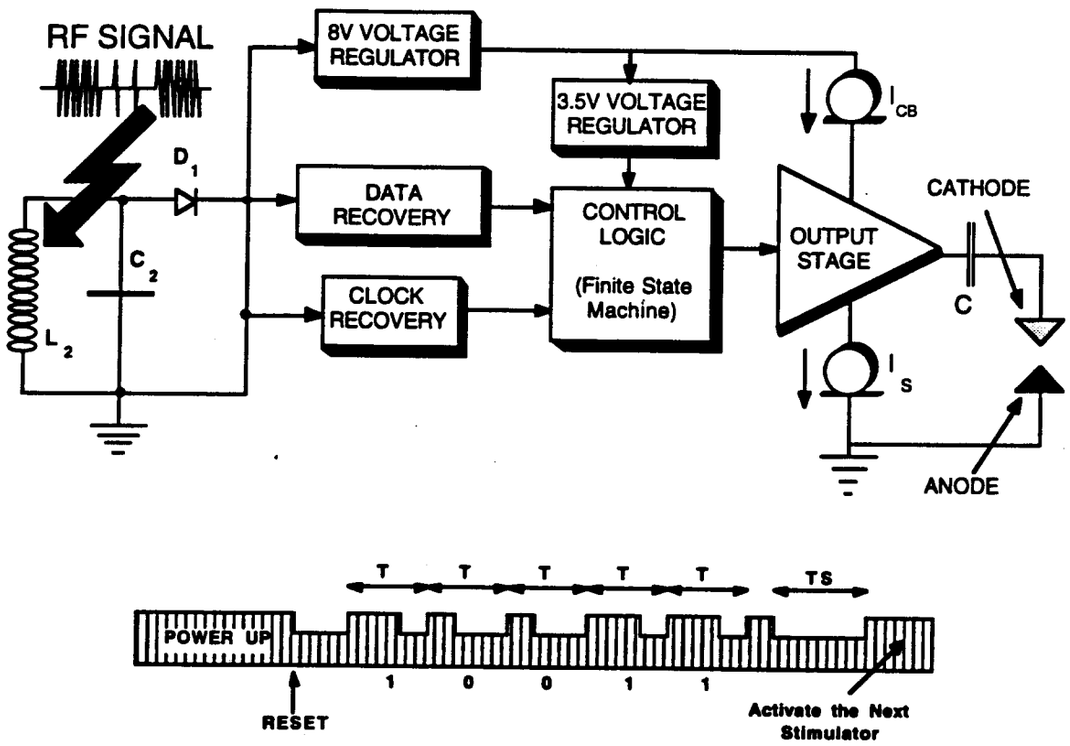

Figure 19: Overall system architecture for the microstimulator circuitry along with the data and power transmission protocol used for the RF telemetry link.

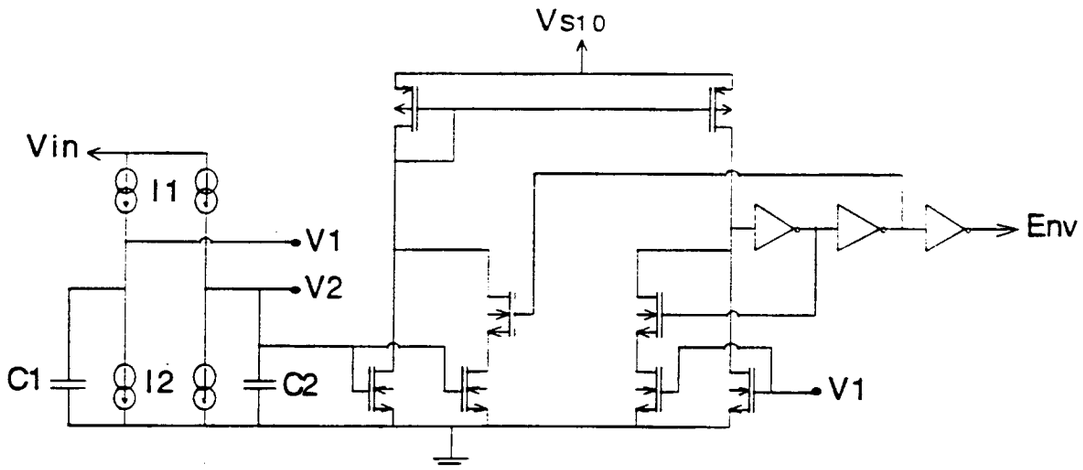

Figure 20: Current mode envelope detection circuitry.

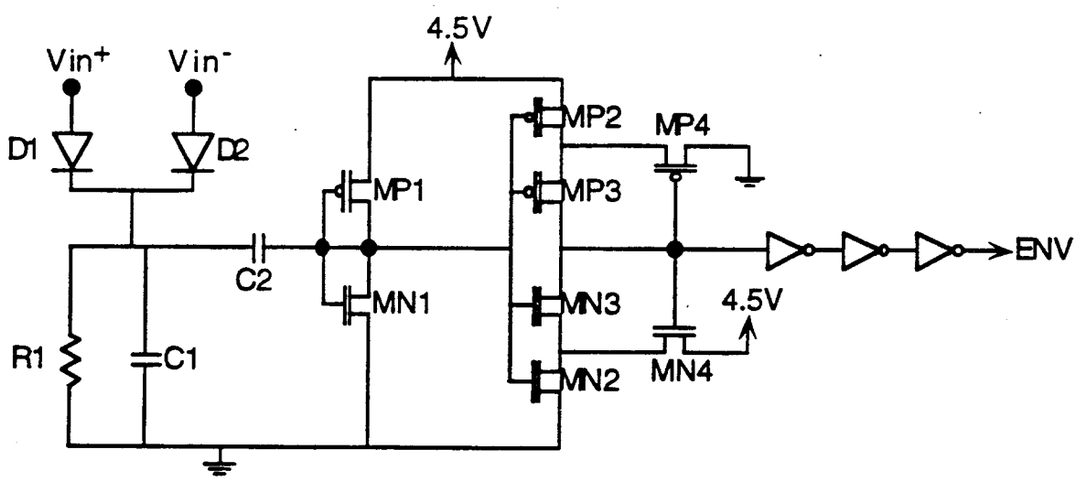

Figure 21: Envelope detection circuitry using high pass and low pass filters.

Figure 20 shows a differential mode envelope detector utilized in this design. The main advantage of this design used to be its smaller size. The first generation design required a very high value resistor in its high pass filter design (≥500kΩ). This resistor required a large die area to lay it out. The design shown in Figure 20 uses current sources I_1 and I_2 to charge and discharge capacitors C_1 and C_2. The capacitors have different values and will charge and discharge at different rates. This will produce a differential voltage that is sent into a schmitt trigger and then a series of inverters to detect the envelope of the input.

For the circuit in Figure 21, the received input signal is first full-wave rectified using the diodes D1 and D2. Then, the signal is fed to a low-pass RC filter formed through R1 and C1 which detects the envelope of the RF carrier and filters out the high-frequency components. The output of this filter is now fed into a high-pass RC filter formed through C2, MN1, and MP1 to bring the DC level of the voltage to ≈2.25V, one half the value of the 4.5V supply. This is

necessary in order to avoid exposing the input of any MOS circuitry to high voltages which may cause a breakdown of the device. In this design the MOS devices MN1 and MP1 are used instead of a large value resistor for the high-pass filter. These transistors are sized to provide an impedance similar to a several hundred kΩ resistor, without consuming the large area that such a resistor would require. The output of the high-pass filter is now fed to a schmitt trigger, formed by MN2-4 and MP2-4, which cleans up the signal and generates sharp pulses. The threshold voltages of the schmitt trigger are set to 1V and 3.5V so that any signal below 1V is considered low, and any signal above 3.5V is considered a logic high. The output of the schmitt trigger is now passed through three inverters which generate the true envelope of the RF carrier.

The results given in the last report were for the envelope detection circuitry shown in Figure 20. During this quarter, more complete testing of each of these circuits has been accomplished, and the results are very good. Both circuit blocks were tested to determine several parameters: the minimum received modulation depth for good envelope detection; the necessary modulation depth for good envelope detection throughout the entire operating range; the operating range of the detector in terms of peak amplitude of the input voltage; the minimum pulse width (in time) that can be detected; and the propagation delay from when the transmitter sends a pulse and when it is detected. The results of these tests for the two different circuits are given in Table 7.

Table 7: Results of testing the envelope detection circuits of Figure 20 and Figure 21.

Property measured in receiver circuitry	***Circuit of Figure 20***	***Circuit of Figure 21***
Absolute minimum envelope modulation to be detected	2V	2V
Minimum envelope modulation that can be reliably detected over entire operating range	5V	2.5V (5V)
Minimum received peak input voltage for proper operation	9V	10V (7V)
Maximum received peak input voltage for proper operation	19V	No Maximum
Minimum pulse length necessary for detection	5µsec	15µsec
Maximum propagation delay (High to Low)	7µsec	9µsec
Maximum propagation delay (Low to High)	8µsec	8µsec

There are some details contained in Table 7 that must be explained in more depth. First, some of these values can be slightly misleading since they can depend largely on the risetime and falltime of the transmitted envelope. In all of these tests a standard class E transmitter, operating at 1.8MHz, was used. The risetime and falltime of the transmitter envelope was ≈15µsec. If a transmitter was used that had faster rise and fall times, some of the measured minimum values could be improved. The absolute minimum envelope modulation that can be detected for each circuit is listed at 2V. This value is determined by the schmitt trigger and can be altered through laser cutting of metal links included in this portion of the circuit. For the operating range, the circuit of Figure 21 is better than Figure 20. The circuit of Figure 21 can operate over a range of 10V minimum, with no maximum and a 2.5V modulation depth. If the modulation depth is increased to 5V, the operating range can extend down to 7V minimum for Figure 21. For the circuit of Figure 20, the range of operation is from 9V minimum to 19V maximum and requires a modulation depth of at least 5V in order to perform reliably over this entire range. Overall, the results obtained from tests on the circuit of Figure 21 appear much better than those from Figure 20.

The circuitry for the complete single channel microstimulator has been again tested this quarter, including testing with the telemetric link. In previous fabrication runs, our biggest problem had been in obtaining reliable functioning of the envelope detection circuitry. In this fabrication run, the design includes two separate envelope detection circuits, and tests so far show that both work well, with the circuit shown in Figure 21 demonstrating a larger range of operation and less variation from die to die in tests to date. In testing the most recently completed Bi-CMOS wafer, many fully functional single channel microstimulator dies have been identified. This wafer is presently undergoing final preparations that are necessary before it can be packaged for implantation. These preparations include: deposition and patterning of a passivation layer over the first metallization layer; deposition of a second metal layer for bond regions; dicing the wafer to obtain the individual devices; and affixing the coil and capacitor to the individual dies. The passivation layer over the first layer metal is required so that the metal does not get shorted out when the coil and capacitor are bonded to the device. The second layer of metal is going to be used in order to provide a thicker, more durable metal pad when trying to bond the receiver coil to the circuit chip. AS was discussed in the previous section, the thicker electroplated pads are much more suitable for microwelding than the aluminum pads. The electroplating step is necessary for forming the on-chip transmitter coil for the multi-channel microstimulator anyway, and will not require any additional processing for μstim-1. During this quarter we finished the mask layout for these layers, obtained masks and have started the processing of the wafer to include the passivation layer and the thick electroplated layer on the wafers. Once this is completed, we will have a number of dice for μstim-1 ready for use in assembling complete devices during the first week in May.

2.2.2 Multi-Channel Microstimulator

Over the past quarter there has been much more extensive testing of all circuit blocks of the multichannel microstimulator. We have been able to test the clock, voltage regulators, envelope detector, power-on reset (POR), control circuitry, output pulse generation circuit, and on-chip transmitter so far. All of these circuits have produced very good results. The clock, voltage regulators and transmitter results were discussed in the last report. Each of these circuit blocks is working as designed. The envelope detection circuit is the same as the one reported for the single channel microstimulator. This circuit is working well, and Figures 22-24 show the envelope detection circuitry working properly with a telemetrically received input envelope of varying pulse durations. This report will discuss the details of testing the Power-on reset circuitry, control logic, and output pulse circuit.

Figure 25 shows a system block diagram of the multi-channel microstimulator along with the data transmission protocol. Each microstimulator initially powers up in its RESET mode. Additionally, any time the data transmitted does not match what the device expects, due to transmission errors or reception of an address that does not match its programmed address, the device returns to its RESET mode and waits for the start of new data transmission. At the start of data transmission the carrier envelope will go low for a set period of time to indicate that data transmission is about to begin. After sending this start-up signal, the address of the microstimulator that is being selected is transmitted along with a parity check. If the received address matches the address that is programmed internally to a given microstimulator, it will respond by transmitting back the data it just received. All other microstimulators will RESET. Once the external circuitry receives the transmission from the selected microstimulator, it can send either a CONTINUE or RESET signal by allowing the envelope to stay low for the desired length of time for either function. If a CONTINUE is transmitted, any further information can be sent, such as the function to be performed, the stimulation pulse duration and amplitude, the selection of the stimulating electrodes, etc. After this additional information is sent, the on-chip

transmitter is used to send back the information that was just received by the device. This ensures that any errors in transmission are detected and allows for a more fault tolerant device. Once again, the external controller can either allow the device to CONTINUE or force it to RESET. If the device is allowed to CONTINUE, it will perform the proper stimulation or circuit/package self-test and then automatically RESET.

To guarantee each device starts in the RESET state, the Power-on reset (POR) circuitry sends a RESET signal to the control logic for the first ≈130μsec after the 4.5V regulator first turns on. The Power-on reset (POR) circuitry has been determined to be operating as it was designed, and the output of the POR circuit in response to an input voltage is shown in Figure 26. In order to keep such a strict data transmission protocol, the control circuitry incorporates a 10 bit counter that is used to time all envelope transitions. The output of the counter is fed into another block, the "counter logic," that determines what the counter value should mean. There are 6 possible states for the output of the "counter logic," and they are shown in Table 8. Figure 27 shows a more detailed view of the start-up protocol of data transmission for this device, depicting a correct and several incorrect data transmission start-up sequences. Both the 10 bit counter and the "counter logic" have been verified to be operating as designed. One further note is that the clock circuitry for the multichannel microstimulator contains links that can be cut in order to allow it to operate at either 1 times, 0.5 times, or 0.25 times the carrier frequency. This means that each counter value can correspond to either 0.56μsec, 1.11μsec, or 2.22μsec for a carrier frequency of 1.8MHz.

The complete logic control circuit has been tested and is working precisely according to specifications. Figure 28 and Figure 29 show an output pulse being delivered across a 330Ω load for a proper input data stream. First the start-up signal (envelope low), device address, function, stimulation pulse amplitude, and a parity bit are sent to the device. The external transmitter waits with the envelope high while the device transmits that data back out, and then a continue signal is sent along with the electrode selection and pulse duration. The external transmitter waits again for the data to be transmitted back out, and then it sends the continue signal, at which point the device sends a stimulation pulse to the proper electrode for the selected time and amplitude. Figure 30 shows a picture of the signal that is sent from the logic circuitry to the on-chip transmitter when a proper input signal has been received, and Figure 31 shows a more blown up picture of this signal. It can be seen that the logic is sending back the same information that it has just received.

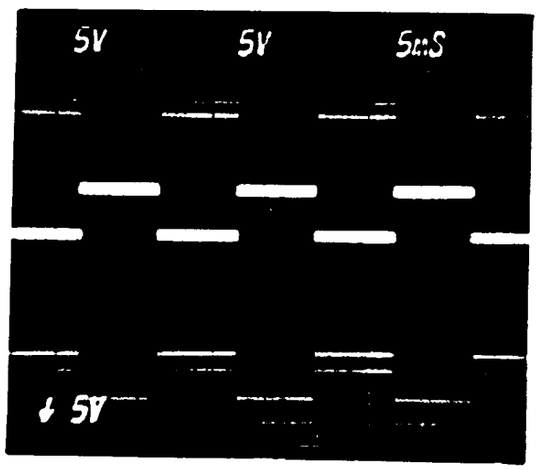

13V-18V Received Input Envelope

Output of Envelope Detection Circuitry

Figure 22: Received input signal with amplitude modulation and output of the on-chip envelope detection circuitry for multi-channel microstimulator.

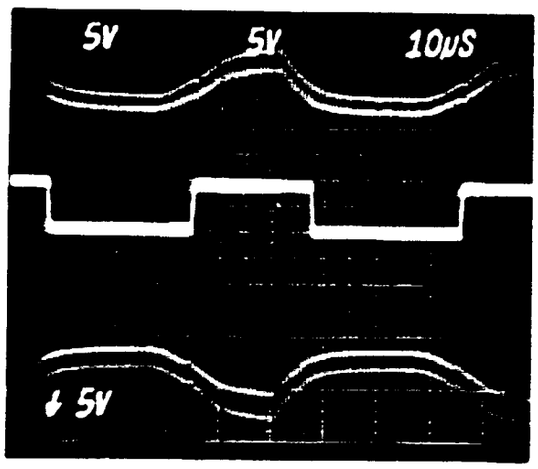

13V-18V Received Input Envelope

Output of Envelope Detection Circuitry

Figure 23: Received input signal with amplitude modulation and output of the on-chip envelope detection circuitry for multi-channel microstimulator.

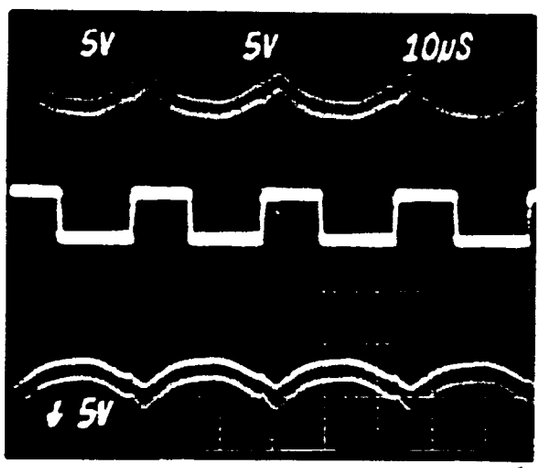

13V-16V Received Input Envelope

Output of Envelope Detection Circuitry

Figure 24: Received input signal with amplitude modulation and output of the on-chip envelope detection circuitry for multi-channel microstimulator.

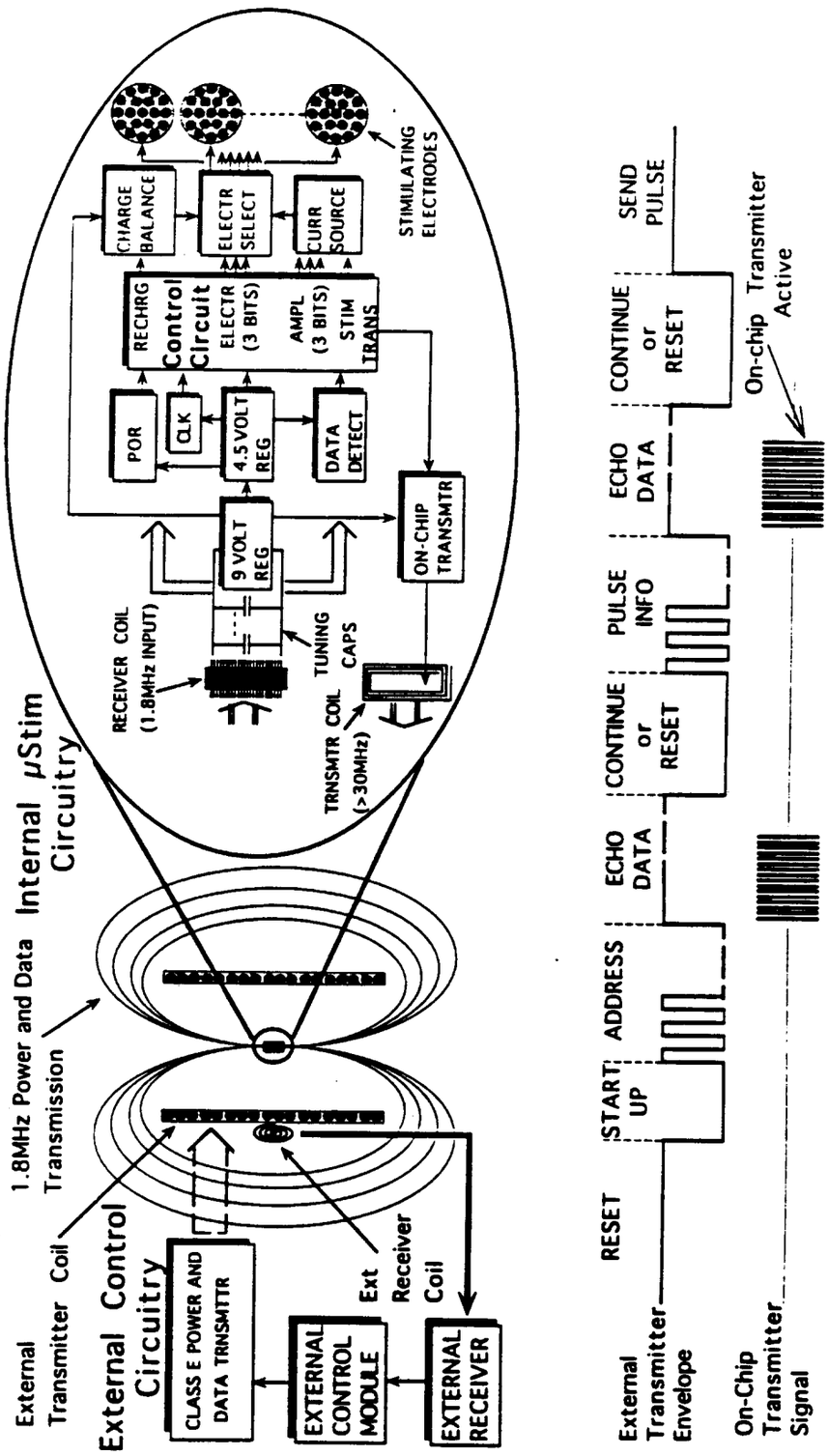

Figure 25: Overall system block diagram and data transmission protocol for a fault-tolerant multichannel microstimulator system with bi-directional telemetry.

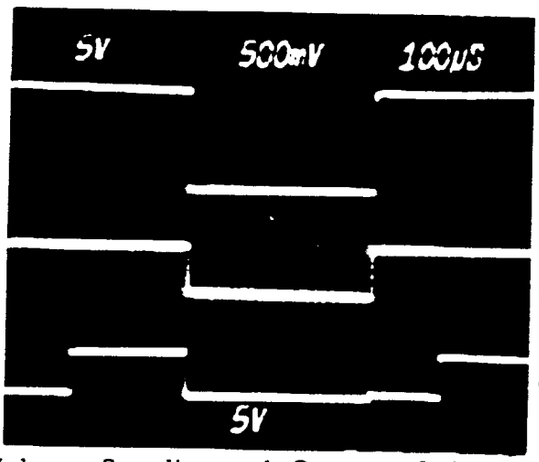

10V Input Voltage

Output of 4.5V Regulator

Output of POR Circuit

Figure 26: Voltage Supplies and Output of the POR Circuit for the Multi-Channel Microstimulator.

Table 8: Counter value and the state it corresponds to for the data transmission protocol in the multichannel microstimulator.

Counter Value (# of clock cycles)	Counter Logic State	
0 to 47	0	Start of Bit = 1 (Envelope time high)
48 to 95	1	Start of Bit = 0 (Envelope time high)
96 to 127	2	Total length of a Bit (Time high + time low)
128 to 191	3	Length of CONTINUE OK signal
192 to 255	4	Length of Start-Up signal
256 +	5	Automatic RESET regardless of state of microstimulator

The output circuitry for the multichannel microstimulator has also been shown to be functioning properly. The amplitude programmability for this circuit was designed to be 3 bit programmable. Table 9 shows the results obtained from testing this circuit. It shows that the circuit can provide from 0-11 mA of current at 7 discrete steps averaging 1.6mA for each step. The value of this step does start out larger and decrease as the absolute value of the pulse amplitude increases, instead of remaining constant. This is likely due to series resistance in the switches that turn the current pulse on and off. Overall, though, the multiamplitude programmability has been tested to be working as it should. The multichannel capability has also been tested, and any of 8 different channels can be selected for stimulation for a single data transmission sequence. The pulse duration capability has been checked, and the absolute minimum pulse duration has not been measured yet, but from the relative turn-on and turn-off times that have been observed, we should be able to vary to pulse duration from <5µsec to a counter time of 255. As was stated previously, this counter time of 255 can correspond to an actual time of 142-567µsec, depending on the clock speed.

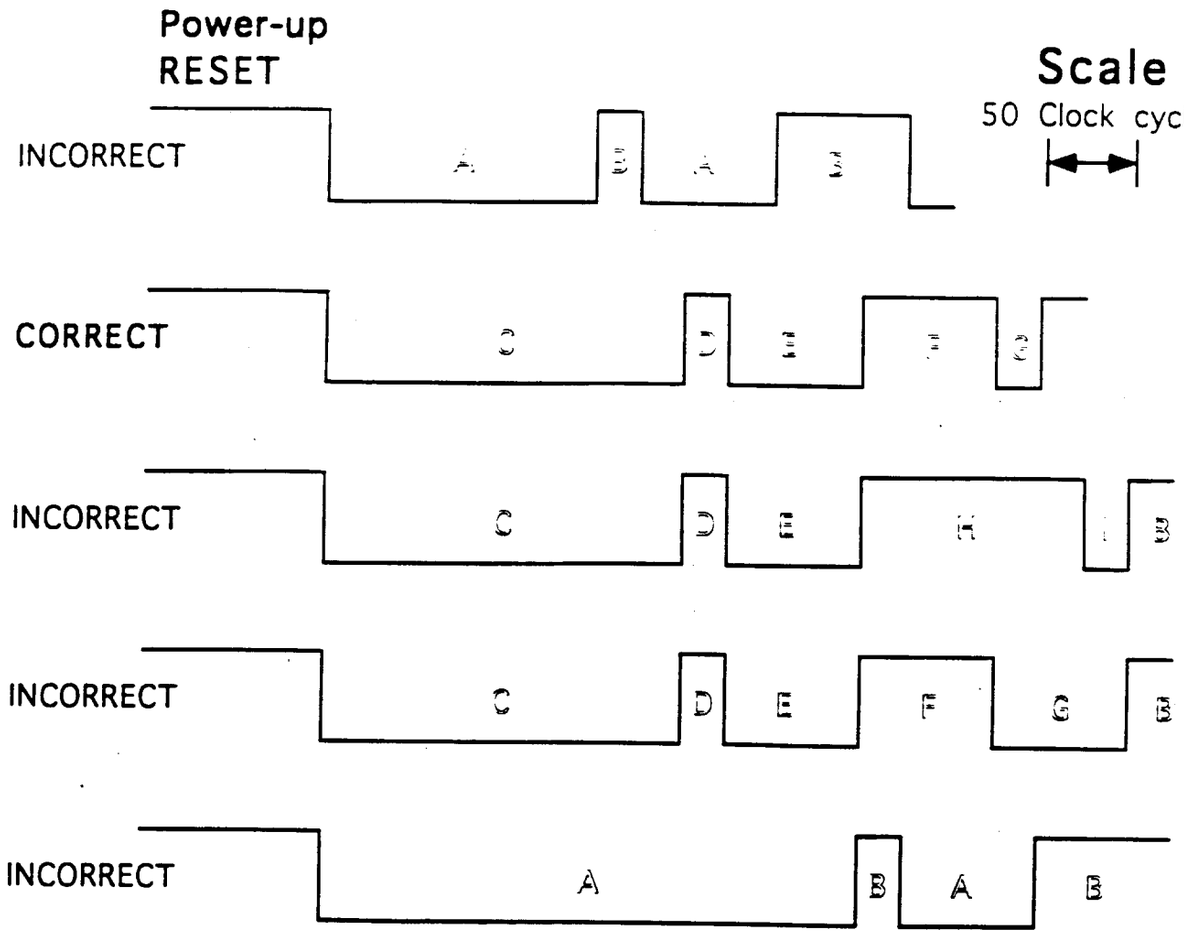

A - Incorrect time period for start-up signal. Return to RESET.

B - RESET mode: wait for start-up signal.

C - Correct time period for start-up signal. Start receiving data bits.

D - Correct time period for start of Bit=1.

E - Correct time period for total length of bit. (time high plus time low) Record the Bit=1.

F - Correct time period for start of Bit=0.

G - Correct time period for total length of bit. (time high plus time low) Record the Bit=0.

H - Incorrect time period for start of data bit. There was a data transmission error.

I - While envelope is low, stay in wait state before RESET.

J - Incorrect time period for total length of bit. (time high plus time low) Return to RESET.

Figure 27: Detailed view of the protocol for the start-up sequence of data transmission for the multichannel microstimulator.

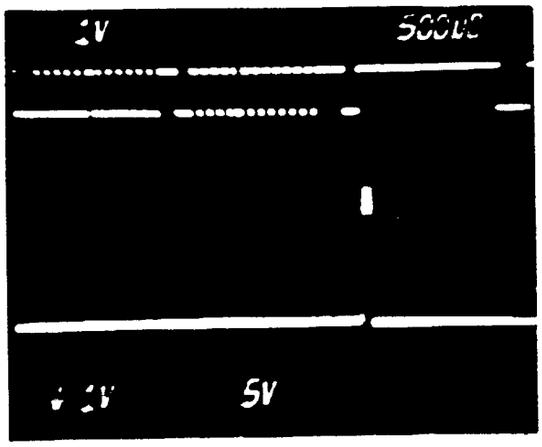

Input Envelope

Output of Constant Current Stimulation

Figure 28: Output voltage across a 330Ω load (≈7mA) of constant current stimulating circuit for multi-channel microstimulator with an input of 111110111111-CONTINUE-000010000000 (Clock logic = 1MHz).

Function	= 11 (Stimulation Mode)
Pulse Amplitude	= 111 (Amplitude = 10mA)
Parity	= 0
Address	= 111111
Electrode Select	= 000 (Electrode #0)
Pulse Duration	= 01000000 (128μsec)
Parity	= 0

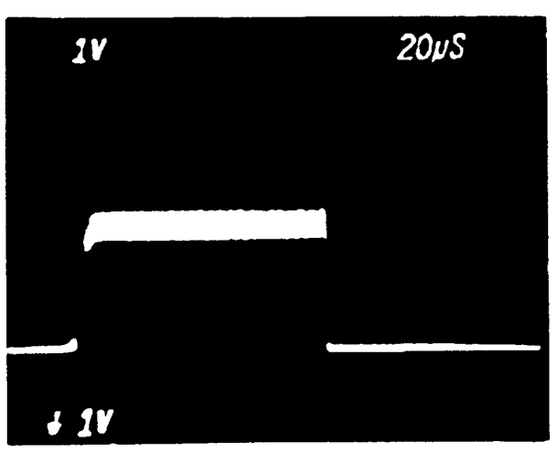

Output of Constant Current Stimulation

Figure 29: Output voltage across a 330Ω load (≈7mA) of constant current stimulating circuit for multi-channel microstimulator with an input of 111110111111-CONTINUE-000010000000 (Clock logic = 1MHz).

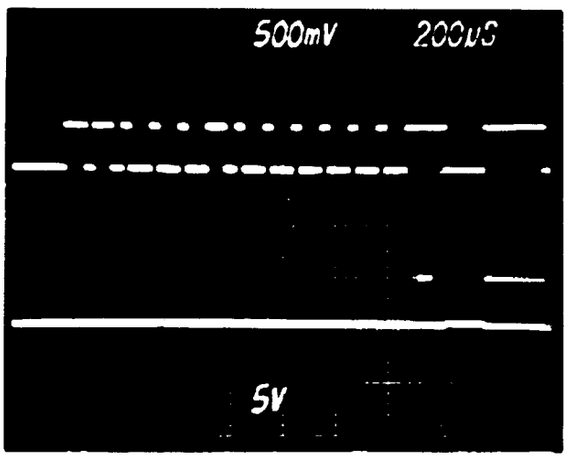

Figure 30: Output signal to on-chip transmitter from logic circuit for multi-channel microstimulator for an input of 001110111111 (clock logic = MHz).

Function	= 00 (Self Test Mode)
Pulse Amplitude	= 111
Parity Bit	= 0
Address	= 111111

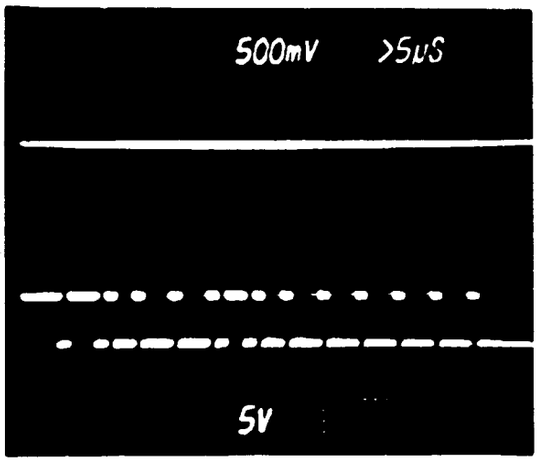

Figure 31: Blown up output signal to on-chip transmitter from logic circuit for multi-channel microstimulator for an input of 001110111111 (Output is echo of input, clock logic = 1MHz).

Table 9: Results of testing the amplitude programmability of the output pulse circuitry for the multichannel microstimulator.

Amplitude Bits	*Measured Amplitude (mA)*
000	0
001	2.1
010	3.9
011	5.8
100	7.3
101	8.5
110	9.7
111	10.9

Every circuit block for the multichannel microstimulator has now been tested and all have been working properly. However, many of these circuit blocks contain programmable links that can be cut with a laser trimmer, and there is still a lot of testing that should be done in order to determine the optimum settings for all the programmable links. Over the next quarter, we will continue testing of these circuit blocks to determine these optimum settings. Also, similar to the single channel microstimulator, the multichannel microstimulator must have a passivation layer deposited over the first layer metal, and the second layer metal must be deposited both for the bonding pads and for the on-chip transmitter coil. This second layer metal will be the thick electroplated structure for additional durability and low resistance.

3. PLANS FOR THE COMING QUARTER:

Our activities for the coming quarter will proceed in several areas. First, we will focus our activities on starting soak test using the new glass packages and silicon substrates. The ultrasonically machined capsules seem very promising and provide a good bond to silicon. We will start accelerated soak tests at a number of temperatures using these capsules in saline. The soaking of our present packages will continue so that we can hopefully obtain a more accurate MTTF. The accelerated temperature will be complemented by additional tests to determine the failure modes and to isolate various leakage paths into the package. We will discuss our approach in this regard in future reports. We will start a new set of in-vivo implants both here at Michigan and at Vanderbilt University. We have prepared a number of good packages for Vanderbilt and will be shipping them these packages in the near future. The in-vivo tests will be very valuable in determining the biocompatibility of the packages. Package testing both in-vitro and in-vivo will be of the highest priority this summer.

We hope to be able to ship the first set of complete microstimulators in the next few months. We have completely functional chips and are now waiting for the completion of a few extra processing steps needed to electroplate the bonding pads and to add a passivation layer on top of the chip before we can assemble complete devices. The multichannel microstimulator designs are also functional and we hope to be able to complete the testing and characterization of these devices also.

4. PUBLICATIONS DURING THE PAST QUARTER

The following papers were prepared and accepted for presentation. A copy of these papers is included with this report.

1. M. Nardin, B. Ziaie, J. Von Arx, A. Coghlan, M. Dokmeci, and K. Najafi, "An Inductively Powered Microstimulator for Functional Neuromuscular Stimulation," Presented at the *13th International Symposium on Biotelemetry*, Williamsburg, VA, April 1995

2. M. Nardin, and K. Najafi, "A Multichannel Neuromuscular Microstimulator With Bi-Directional Telemetry," *1995 Int. Conference on Solid-State Sensors and Actuators, Transducers '95*, to be Held in Stockholm, Sweden, June 1995

3. Hermeticity Testing of Glass-Silicon Packages with On-Chip Feedthroughs," *1995 Int. Conference on Solid-State Sensors and Actuators, Transducers '95*, to be Held in Stockholm, Sweden, June 1995

HERMETICITY TESTING OF GLASS-SILICON PACKAGES WITH ON-CHIP FEEDTHROUGHS

J. Von Arx, B. Ziaie, M. Dokmeci, and K. Najafi

Center for Integrated Sensors and Circuits
University of Michigan
Ann Arbor, Michigan 48109-2122

SUMMARY

This paper reports on hermeticity test results performed on a silicon-glass hermetic package in aqueous environments. The package utilizes anodic bonding of glass to silicon at temperatures below 320°C to form a hermetically sealed cavity large enough to contain hybrid components. Up to 200 sealed polysilicon feedthrough lines can be obtained per mm at the edge of the package. Hermeticity is maintained by planarizing these feedthrough lines, and then depositing a smooth top polysilicon surface for anodic bonding of the glass capsule. Accelerated long term tests indicate a lifetime of at least many years. In-vivo tests in guinea pigs for two months have shown the package to be biocompatible and rugged.

INTRODUCTION

Hermetic packaging with multiple feedthroughs is necessary for a variety of sensors and actuators [1]. Several hermetic packaging techniques currently exist, but few provide reliable feedthroughs in a small volume. Most utilize either various types of welding, or sealants such as epoxies and polymers. However, these techniques tend to leak over time, are not biocompatible, require large tolerances, and are incompatible with low-cost batch fabrication techniques. We have developed a hermetic package based on electrostatic bonding of glass to silicon for an implantable functional neuromuscular stimulator, as shown in Figure 1 [2,3]. The glass capsule is used to protect a circuit chip, a hybrid coil, and a hybrid capacitor from biological fluids, while providing access to the external stimulating electrodes, and is less than 2mm in diameter and 8mm in length. This packaging technology is also attractive for a wide range of applications, including chemical, automotive, bio-medical, oceanic, and vacuum packaged sensors. This package is very small, transparent to radio frequencies (compatible with RF telemetry), transparent to visible light, biocompatible, compatible with discrete components, can be batch fabricated, and has multiple dense feedthroughs. This paper reports on accelerated long term testing results and on several improvements in the technology which have helped increase the package lifetime over our previously published results [2,3].

STRUCTURE AND FABRICATION

The hermetic package utilizes electrostatic bonding of a glass capsule to a silicon substrate containing sealed feedthroughs to form a hermetically sealed cavity. Figure 2 is a diagram showing the basic elements of the package. The #7740 glass capsule is fabricated separately using either standard molding and machining techniques, or using ultrasonic micromachining techniques. The fabrication of the silicon substrate begins with the growth of a thick field oxide over the substrate to provide isolation for the feedthroughs. Then closely spaced polysilicon lines (1μm thick, 2μm spacing) are deposited and patterned to form the feedthrough lines. The surface over the feedthrough lines is planarized with LTO (2000Å) and PSG (≈2.0 μm). The PSG is reflowed at 1100°C for 2 hours to form a planarized surface suitable for electrostatic bonding. A passivation layer of 3000Å oxide, 1500Å nitride, and 3000Å oxide is then deposited on top to prevent direct exposure of PSG to moisture. A second layer of fine-grain polysilicon is then deposited, lightly doped, and patterned to form the bonding surface for the glass-silicon anodic bond. The fine-grain polysilicon is deposited at a temperature of 577°C to minimize surface roughness so that a hermetic seal can be obtained [3], and is lightly doped at 950°C for about 30 minutes (this produces a sheet resistance of a few hundred Ω per square). One has to be careful not to highly dope this film so that the film smoothness can be maintained and to prevent any significant recrystallization. Finally, contacts are opened to the polysilicon feedthrough lines, and metal bonding pads are deposited. This packaging process requires a total of 6 masks.

To improve the lifetime of the package and prevent premature failure due to moisture penetration into the package, one has to make sure that the bonding surface is planar and free of any surface irregularities. Therefore, planarization over the feedthrough lines is very important. Previously we had shown that by reducing the separation

Figure 1: SEM view of a single-channel implantable microstimulator for neuromuscular microstimulation. A glass package is used to hermetically seal the integrated circuit chip, the hybrid chip capacitor and the on-chip coil. Multiple on-chip feedthrough lines interconnect stimulating electrodes with the sealed electronics.

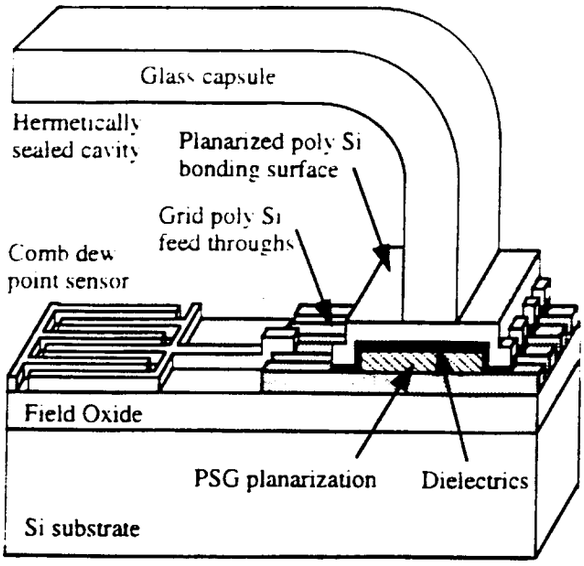

Figure 2: Overall structure of the glass-silicon package with sealed grid feedthroughs.

between two polysilicon lines one can achieve a very planar surface by depositing and reflowing a PSG film [3]. A SEM cross-sectional view of two wide polysilicon feedthroughs lines separated by 1.5μm is shown in Figure 3. As can be seen, although the planarization is very good, one can still observe a dimple of a few hundred angstroms in depth. This could provide a path for moisture penetration inside the package.

In order to improve the planarization process, we have developed a new grid-feedthrough technique. Here, instead of using wide polysilicon feedthrough lines, we use a large number of narrow feedthrough lines that are closely spaced, as shown schematically in Figure 2. The regular structure of the grid reduces the surface non-planarity. To achieve an effective planarization, however, one has to make sure that the feedthrough lines are less than ~4μm wide and spaced at ~2-3μm. This is easily possible using simple optical photolithography and dry etching techniques. Figure 4 shows a SEM cross-sectional view of planarized grid polysilicon feedthroughs. As can be seen the planarization is perfect and the top surface is flat. Another nice feature of the grid feedthroughs is that the planarization is tolerant of variations in width and spacing of the individual polysilicon lines.

In order to prevent the exposure of the dielectric films at the edges of the silicon substrate, where the substrate is diced, we etch the field dielectrics there and use the top polysilicon film to totally shield the dielectric layers. Therefore, the polysilicon film wraps around the dielectric films and contacts the silicon substrate around the entire perimeter of the packaging die. This polysilicon cap prevents moisture from seeping into the field oxide through the sides of the die. Following the fabrication of the substrate and the package, the two are ready for bonding and testing.

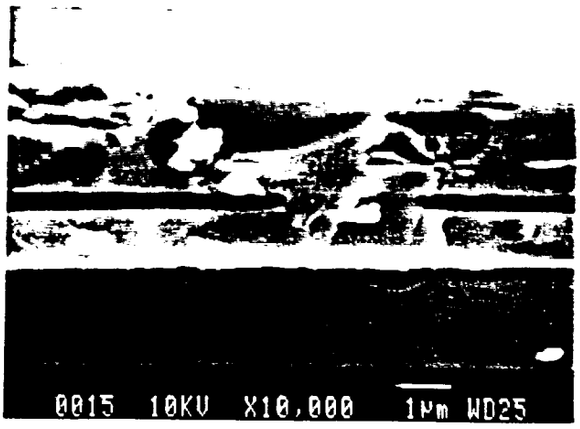

Figure 3: A SEM cross-sectional view of two wide polysilicon feedthroughs separated by 1.5μm. Although the planarization is very good, one can still observe a dimple of a few hundred angstroms in depth.

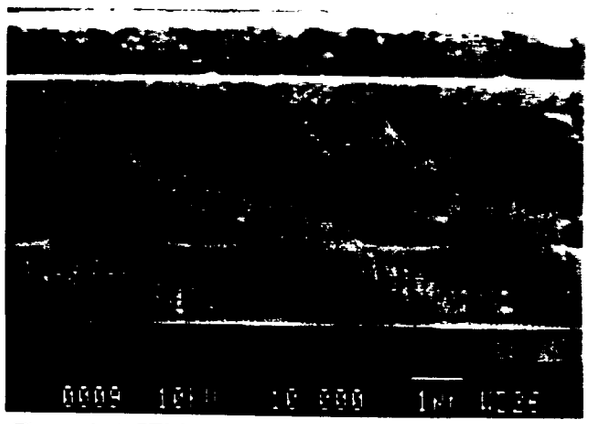

Figure 4: A SEM cross-sectional view of a planarized grid polysilicon feedthroughs. As can be seen the planarization is almost perfect and the top surface is flat.

ELECTROSTATIC BONDING

Electrostatic bonding of glass to silicon is widely used in integrated sensors and actuators [1]. In this process, silicon and glass are heated to between 180-500°C while a DC voltage of 200-2000V is applied between the two, with the negative potential applied to the glass. The result is a permanent chemical bond.

For this application, it is important to keep the bonding temperature below 320°C so that the hybrid components required in the microstimulator are not damaged during bonding. In order to achieve a reliable bond, a voltage of 2000V is applied between the glass capsule and the top fine-grain polysilicon film (the silicon substrate is floating) at a temperature of ≤320°C for about 10 minutes. The high voltage is needed since an appreciable amount of the electric field is dropped in the glass which is about 2mm high. It should be noted, however, that because of the large cavity inside the capsule, the electric field strength does not become large enough to cause damage in MOS devices. However, in order to prevent any possible damage to circuit

components, one can deposit a metal layer on IC chips to shield them from the high electric field. The glass will form a permanent bond to the polysilicon film. This bond is strong enough that it will tear the films off of the substrate when the glass capsule is forcibly removed.

In order to increase the yield of the electrostatic bonding process several factors should be considered. First, the yield of the bonding process increases significantly if the silicon substrate is thinned to ≈100μm. This makes the substrate more conformal to any curvature on the glass capsule. It should be noted that this is a problem when the glass capsules are individually fabricated using either a molding technique or by manually working and polishing them. The second of these techniques was used to form the glass capsule shown in Figure 1. One way to circumvent this problem is to ultrasonically machine the capsules from thick wafers of glass. In this process, a 2mm-thick #7740 glass wafer is machined to create the cavities inside it ultrasonically. Note that these cavities can be of any desirable size determined by the application, and do not go all the way through the glass wafer. After the cavities are created, the wafer is diced using a dicing saw to separate the individual capsules. This new technique allows the use of glass wafers with a much better surface planarity and polish, lowers the cost, and is compatible with batch fabrication. Figure 5 shows a SEM view of a glass capsule fabricated using this technique.

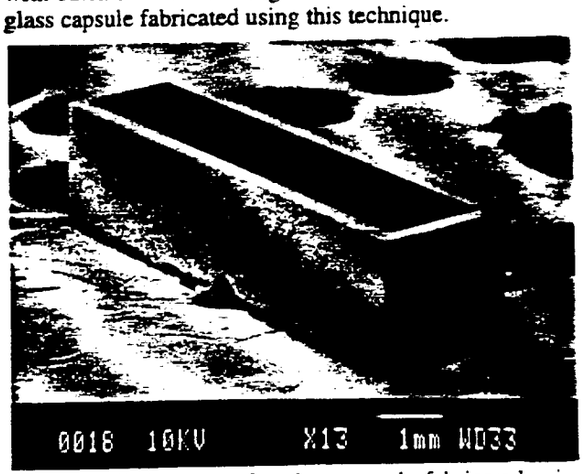

Figure 5: SEM view of a glass capsule fabricated using ultrasonic micromachining and dicing of a 4"-diameter, 2mm-thick #7740 glass wafer.

The second factor that improves the overall yield is the temperature uniformity during bonding. Since the glass package is rather thick, one has to take steps to maintain a constant temperature across the glass-silicon sandwich. This can be achieved by placing the glass-silicon sandwich in an enclosure to prevent any heat loss due to convection. Note that after bonding, the bonded package should be cooled slowly (about 10 minutes to room temperature) to avoid generating large stresses. Third, the glass and silicon need to be extensively cleaned before bonding. Standard solvent cleaning in acetone and alcohol followed by a DI water rinse is sufficient. Finally, we have minimized the bonding time needed for a hermetic seal by sputtering aluminum on the top surface of the glass capsule to help uniformly distribute the applied electric field during bonding. The aluminum coating is removed after bonding by a wet etch. Uniform hermetic bonds are obtained in within 10 minutes.

The yield of this packaging technique is now 85% (yield is defined as the percentage of packages which last more than 24 hour soaking in DI water). The 15% loss of the packages is due to poor bonding alignment, lithography defects, and glass capsule defects. The packages that fail this initial screening are not subjected to further accelerated tests.

ACCELERATED TESTS

These packages have been tested in a variety of environments, including DI water, saline, and in animals. Temperature-accelerated soak tests have been performed primarily in DI water.

Moisture penetration inside the package is monitored either visually or using integrated on-chip dew-point sensors. The dew point sensors are interdigitated metal comb patterns which undergo a large impedance change when moisture condenses on them. For the lifetime studies reported here, we define package failure as condensation at room temperature, which corresponds to <5% relative humidity (RH) at a soaking temperature of 95°C, and <10% RH at a soaking temperature of 85°C.

The packages have been subjected to temperature-accelerated tests in DI water at 85°C and 95°C. Every few days the packages are individually removed from the soaking solution, allowed to cool to room temperature, visually examined for condensation or damage, and electrically probed to measure the response of the dew point sensors. Generally we are able to measure condensation electrically a few days before we can observe it visually. Tables 1 and 2 summarize the results from these long term soak tests to date, although the tests are still on-going for some of the packages.

Table 1: Key data for 95°C soak tests in DI water.

Number of packages in this study	10
Failed within 24 hours (number discarded)	1
Packages lost due to mishandling	2
Longest lasting packages so far in this study	227 days
Packages still under test with no sign of room temperature condensation inside	2
Average lifetime to date (MTTF)	*90 days*

Table 2: Key data for 85°C soak tests in DI water.

Number of packages in this study	10
Failed within 24 hours (number discarded)	2
Packages lost due to mishandling	3
Longest lasting packages so far in this study	221 days
Packages still under test with no sign of room temperature condensation inside	4
Average lifetime to date (MTTF)	*116 days*

Several points should be made with regard to the above data. First, the failure of the packages that leak after a few days is due to misalignment of the glass

capsule, and/or defects on the surface of the glass or silicon substrate. Second, many of the packages that failed in both of these tests were lost due to excessive handling and not because of the failure of the package itself (at least 3 packages in the 85°C test and 2 in the 95°C test are known to have leaked immediately after being dropped). Third, we have repeatedly observed in saline-soaked high temperature tests that the silicon substrate dissolves away slowly causing a failure. Dissolution rates of up to a few microns per day at 95°C in saline have been measured. The dissolution rate of silicon in DI water is much smaller and does not effect the package significantly, and has allowed us to obtain the above results. It should be noted that the dissolution of silicon in saline is much slower at body temperature and will not be a major issue in biomedical applications. Fourth, it should also be noted that corrosion of the thin films used can be a cause for failure, although we have not observed any corrosion effects in these packages yet. Finally, the continuous cooling and heating of the packages when they are pulled out of the soaking solution for testing causes an unnecessary stress on the package which may cause premature failure. In spite of these problems, the above data shows that these packages have lasted for a very long time in DI water. In order to predict the lifetime of the package, one needs to determine mean-time-to-failure (MTTF) and the activation energy (Q).

The acceleration of the soak tests can be modeled as an Arrhenius process which is described by MTTF = A exp(-Q/kT). Ironically, we cannot accurately extrapolate a value for Q and MTTF from our data so far because many of the packages have not failed yet! Some of our preliminary tests on similar packages produced an activation energy Q of ≈0.946 eV [3]. Using this value and the approximate MTTF indicated in the tables above, one can calculate an average lifetime of about 50 years at body temperature (37°C). We caution, however, that the lifetime is a strong function of Q, and until Q can be accurately determined for our current package, the above values are subject to change. It should be noted that in spite of this uncertainty at this point, the activation energy of 0.946eV is rather conservative and is lower than that measured for some packages used by the IC industry.

Soak tests on these packages are also being performed in saline at room temperature, as summarized in Table 3. So far, out of 6 packages tested at room temperature, one leaked within 24 hours (infant mortality) and none of the remaining 5 have shown any sign of moisture penetration after 120 days of soaking.

In addition to in-vitro tests, four of these packages have been implanted in guinea pigs for two months and then explanted. The devices were placed on top of the dura, in an area where the skull had been cut away. The skin was then sutured together, leaving the devices sitting on top of the dura, not fixed in place. After 2 months in-vivo three of these packages showed no signs of leakage, and one had fluid inside of it, probably due to damage in handling. In all three cases, healthy tissue had regrown up around the glass package. There was no sign of infection, and no visible tissue abnormalities, clearly indicating the biocompatibility of the materials used.

Table 3: Data for room temperature saline soak tests.

Number of packages in this study	6
Failed within 24 hours (number discarded)	1
Longest lasting packages so far in this study	120 days
Number that do not yet have measurable room temperature condensation inside	5
Average lifetime to date (MTTF)	*105 days*

CONCLUSION

A hermetic package suitable for integrated sensors and actuators has been described. This package utilizes electrostatic bonding of a #7740 glass capsule to a silicon substrate and is small, can be batch fabricated, and provides hundreds of sealed feedthroughs. Accelerated long term tests of the device have been performed in DI water at 95°C and 85°C, and are still ongoing. The data collected so far indicates an expected lifetime of at least many years at body temperature. Non-accelerated tests in saline are also on-going, and show no moisture penetration of the package. Initial *in-vivo* tests have shown that the device is rugged enough to withstand the harsh environment of the body. A study of the failure modes of the package is underway. The glass capsule, the silicon substrate, and the thin films are all excellent barriers to moisture penetration and should last for many decades. Dissolution and corrosion of the various thin films, and moisture penetration at the glass-silicon interface are some of the most important failure modes for the package.

ACKNOWLEDGMENTS

The authors wish to thank Dr. F.T. Hambrecht and Dr. W.J. Heetderks of the National Institute of Health for their guidance and encouragement. We would also like to thank Dr. Michael W. Putty and the General Motors Research and Development Center, Warren, Michigan, for help in PSG and LTO deposition. We also thank Mr. Jim Wiler and Mr. Pete Finger for help with animal testing. This work was supported by the Neural Prosthesis Program, NIH, under contract number NIH-NINCDS-N01-NS-4-2319.

REFERENCES

[1] W.H. Ko, J.T. Suminto, and G.J. Yeh, "Bonding Techniques for Microsensors" *Micromachining and Micro-packaging for Transducers*, Elsevier Science Publishers, B.V. 1985

[2] B. Ziaie, M. Nardin, J. Von Arx, K. Najafi ,"A Single Channel implantable Microstimulator for Functional Neuromuscular Stimulation", *Proceedings, 7th Int. Conf. on Solid State Sensors & Actuators*, Yokohama, June 1993, pp. 450-453

[3] B. Ziaie, J. Von Arx, M. Nardin, K. Najafi, "A Hermetic Packaging Technology with Multiple Feedthroughs for Integrated Sensors and Actuators", *Proceedings, 7th Int. Conf. on Solid State Sensors & Actuators*, Yokohama, June 1993, pp. 266-269

A MULTICHANNEL NEUROMUSCULAR MICROSTIMULATOR WITH BI-DIRECTIONAL TELEMETRY

M. Nardin and K. Najafi

Center for Integrated Sensors and Circuits
EECS Department, University of Michigan
Ann Arbor, Michigan 48109-2122

SUMMARY

This paper presents a multichannel implantable microstimulator to be used for functional neuromuscular stimulation (FNS). The microstimulator receives power and data through wireless RF telemetry and incorporates voltage regulators, clock recovery, data detection, output drivers, and an active on-chip transmitter onto a single BiCMOS IC chip measuring 1.4mmx13.5mm and dissipating only 40mW of power. The chip can deliver programmable amplitude (1-10mA) and duration (1-256μsec) current pulses into tissue through eight on-chip electrodes. An on chip transmitter and integrated coil allow data transmission out on an AM modulated 33MHz RF carrier for closed-loop system control.

INTRODUCTION

FNS has been used to successfully restore function in a variety of applications, including stimulation of paralyzed muscle [1]. We have developed and previously presented work on a small implantable *single-channel* microstimulator for neuromuscular stimulation [2]. This original device has been a major improvement over previous systems in size and functionality. However, many future implantable systems require even higher performance levels in terms of their user programmability, power requirements, number of stimulation channels, and improved reliability. As reported by *Soma* [3], one of the most important features for implantable devices is reliability since these devices cannot be easily monitored and failure would involve surgery and cause mental trauma to the patient. For improved reliability, for monitoring the integrity of the packaged device, and for detecting errors in data transmission it is also very important to add a telemetry link back from the implant to the outside world that would allow the implant to alert the external control system of any malfunctions. Many future devices also need to provide the user with a greater range of programmability of the pulse duration and amplitude, should consume much less power, and should be capable of delivering electrical stimuli through a number of channels to achieve greater spatial resolution and selectivity. The multichannel microstimulator reported here achieves these goals in a single integrated chip fabricated using a BiCMOS technology and employing novel circuits and microfabrication techniques.

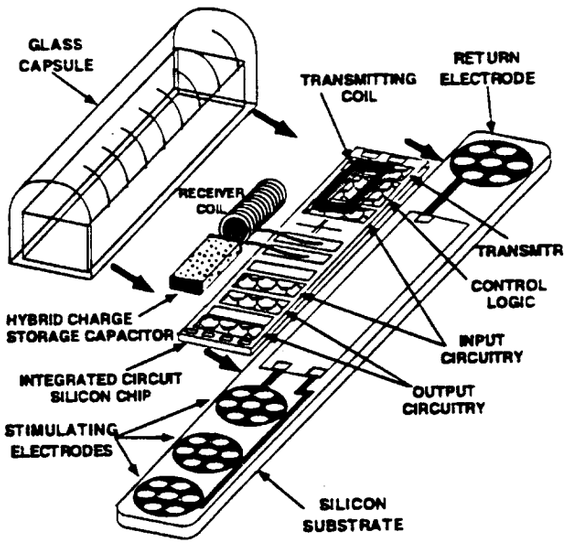

Figure 1: Overall structure of the multichannel microstimulator

MICROSTIMULATOR STRUCTURE

Figure 1 shows the overall structure of the multichannel microstimulator. It consists of six discrete elements: a micromachined silicon substrate; a silicon IC chip; a hybrid capacitor used for charge storage of the stimulation pulse; a hybrid receiver coil for power and data reception; an electroplated transmitter coil; and a custom machined glass capsule. The silicon substrate contains one return electrode and up to 8 stimulating electrodes. The IC chip is used for data reception, transmission, and microstimulator control and is affixed atop the silicon substrate. The hybrid capacitor and receiver coil are mounted on the IC chip, while the electroplated transmitter coil is IC compatible and is fabricated on-chip at the end of the BiCMOS process. Lastly, a hermetic package is provided for the microstimulator circuitry and hybrid components by electrostatic bonding of the glass capsule to the silicon substrate.

SYSTEM ARCHITECTURE

Figure 2 shows the overall system block diagram for a multichannel microstimulator with bi-directional telemetry. This system consists of an external control module that operates a class E transmitter for power and data transmission; an internal microstimulator receiver circuitry; an internal active on-chip transmitter; and external receiver circuitry for closed-loop system control. Work on the external power and data transmitter for such applications has been previously presented [4]. The following sections will present the development and results obtained from testing the internal circuitry for the multichannel microstimulator.

1995 Transducers Conference, Stockholm, Sweden

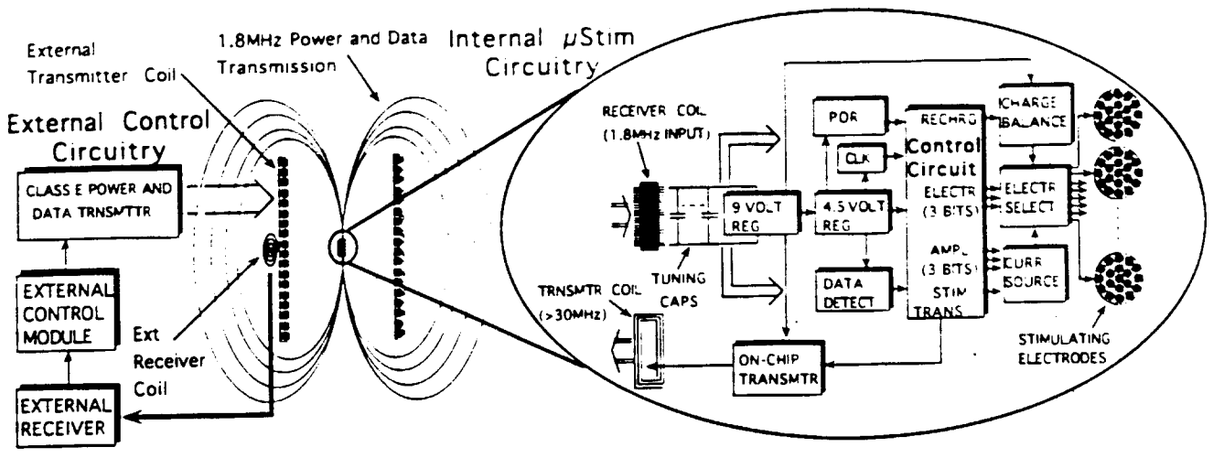

Figure 2: Overall system block diagram for the multichannel microstimulator

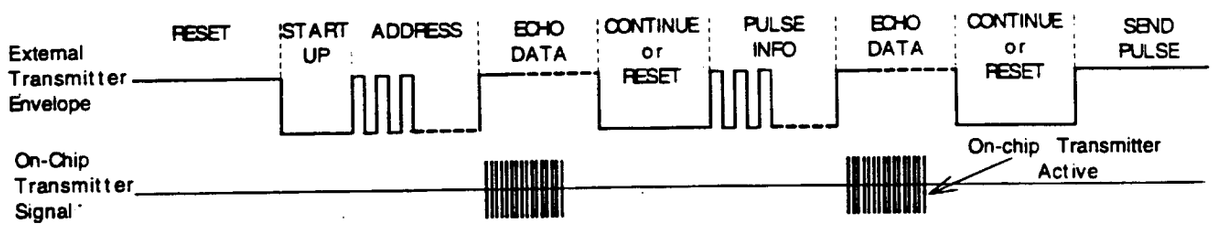

Figure 3: Data transmission protocol for the multichannel microstimulator

MICROSTIMULATOR REQUIREMENTS

The main device requirements of the multichannel microstimulator are small size, broad functionality, low power, and high reliability. The microstimulator should have a diameter ≤2mm in order to be injectable. Many applications of this device will require precise positioning of the stimulating electrodes, which can be satisfied by a multichannel design, and the ability to inject precise packets of charge into muscle tissue to set a desired stimulation level, which requires programmability of stimulation pulse duration and amplitude. The microstimulator also requires parity checks along with a strict data transmission protocol and a bi-directional telemetry link in order to obtain an improved reliability.

DATA TRANSMISSION PROTOCOL

Figure 3 shows the data transmission protocol for the multichannel microstimulator. Each microstimulator initially powers up in its RESET mode. Additionally, any time the data transmitted does not match what the device expects, due to transmission errors or reception of an address that does not match its programmed address, the device returns to its RESET mode and waits for the start of new data transmission. At the start of data transmission the carrier envelope will go low for a set period of time to indicate that data transmission is about to begin. After sending this start-up signal, the address of the microstimulator that is being selected is transmitted along with a parity check. If the received address matches the address that is programmed internally to a given microstimulator, it will respond by transmitting back the data it just received. All other microstimulators will RESET. Once the external circuitry receives the transmission from the selected microstimulator, it can send either a CONTINUE or RESET signal by allowing the envelope to stay low for the desired length of time for either function. If a CONTINUE is transmitted, any further information can be sent, such as the function to be performed, the stimulation pulse duration and amplitude, the selection of the stimulating electrodes, etc. After this additional information is sent, the on-chip transmitter is used to send back the information that was just received by the device. This ensures that any errors in transmission are detected and allows for a more fault tolerant device. Once again, the external controller can either allow the device to CONTINUE or force it to RESET. If the device is allowed to CONTINUE, it will perform the proper stimulation or circuit/package self-test and then automatically RESET. This data transmission protocol includes parity checks along with the bi-directional telemetry link in order to obtain the high level of fault-tolerance and reliability that is desired for bioimplantable devices.

MICROSTIMULATOR RECEIVER CIRCUITRY

The receiver circuitry has been fabricated using a 3μm, 2-poly, single-metal BiCMOS process and is shown in Figure 4. The overall circuit measures 1.4mm by 13.5mm, contains 2800 devices, and consumes ≤40mW power with an AC input voltage of 20V. The microstimulator receives power and data from an amplitude modulated RF carrier through an inductively coupled link. The RF carrier is used to generate regulated

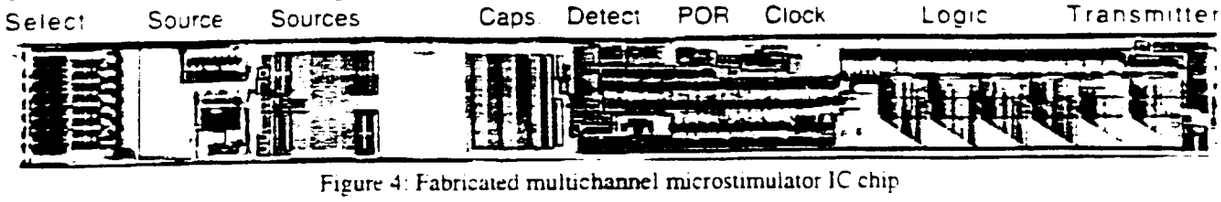

Figure 4: Fabricated multichannel microstimulator IC chip

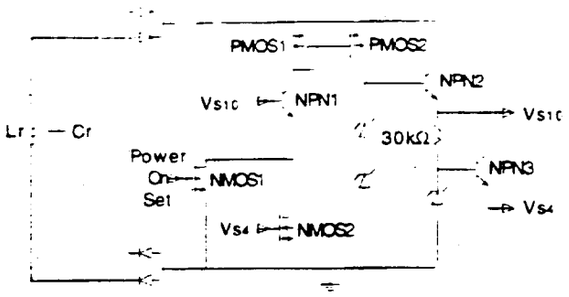

Figure 5: Low Power Consumption Voltage Regulation Circuitry for 10V and 4V Supplies

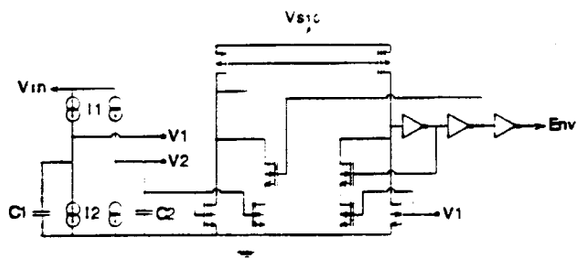

Figure 6: Differential input envelope detection circuitry with active feedback for hysteresis level determination.

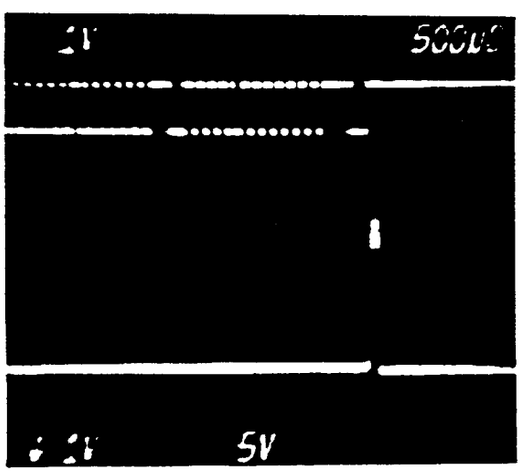

Figure 7: Output pulse being delivered across a 330Ω load after receiving the proper input data stream

4.5V and 10V voltage supplies for the on-chip circuitry and for the output current drivers, generates a clock from the carrier signal, decodes the modulated control data, interprets the control data, generates a programmable constant current output pulse for muscular stimulation when appropriate, and transmits information out through an on-chip transmitter and coil.

Figure 5 shows the circuit diagram for the voltage regulators. NMOS2 acts as a current source with NPN1 as a buffer against high input voltages. This current is mirrored through PMOS1 and PMOS2 to provide a constant current of 10 times the base current of NPN2 through the series zener diodes. Even with large voltage swings across the receiver coil L_r the current through the two zener diodes will remain fairly constant and provide a good DC voltage. The voltage supplies have been measured at 10.23V±0.03V and 4.77V±0.01V for an AC input voltage of 20V and consume <4mW power.

The data decoder, shown in Figure 6, employs a differential input current-mode operation for reliable demodulation in the face of spurious changes in the amplitude modulated carrier. It uses current sources I1 and I2 to charge and discharge capacitors C1 and C2. The capacitors have different values and will charge and discharge at different rates. This will produce a differential voltage that is sent into a schmitt trigger to detect the envelope of the input. Hysteresis levels can be set by the feedback provided from the schmitt trigger, and has been tested to respond to amplitude modulation depths ranging from 0.5V to >5V.

The clock and logic circuitry were designed to operate at a frequency of 2MHz, and have been tested to work at more than 4MHz. The output circuitry was measured to produce current pulses, from any of 8 programmable channels, ranging in time from 1µsec to 512µsec and in amplitude from 1.25mA to 10mA by 1.25mA steps. We have tested the entire system with a telemetric link, and Figure 7 shows an output pulse from the microstimulator circuitry across a 330Ω load, along with the input data that has been received.

ON-CHIP TRANSMITTER

One of the most important features of this device is the active on-chip transmitter, as it allows for bi-directional communication and a much more fault-tolerant system. The on-chip transmitter consists of a coil and active driver similar to the external power/data transmitter. Figure 8 shows the schematic for the on-chip active transmitter. It consists of an inductor L_t for RF-telemetry of data to the outside world, capacitor C_t for tuning the LC resonance of the transmitter coil, tuning capacitor C_{set} for frequency setting of the self-oscillating NAND-inverter-inverter loop, an NMOS drive transistor for driving the inductor, and a transmit signal to the NAND that turns the oscillator on and off. All of the elements of this transmitter are

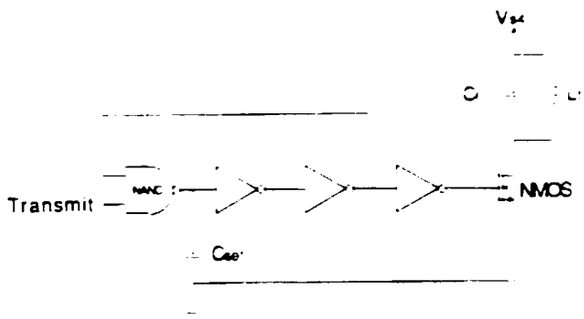

Figure 8: On-chip transmitter circuit design

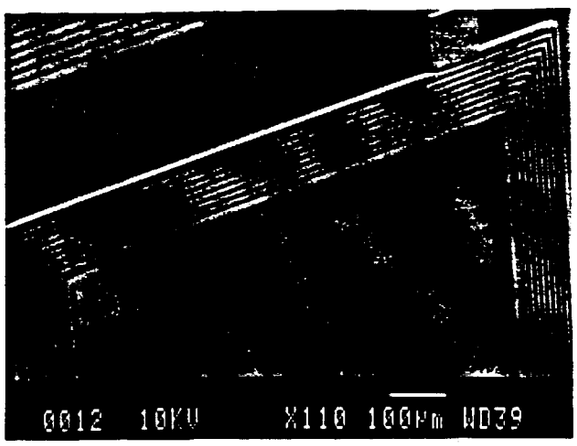

Figure 9: SEM photograph of part of an on-chip electroplated nickel coil for data transmission out. It has a measured inductance of 1.1µH and a self resonance of >40MHz.

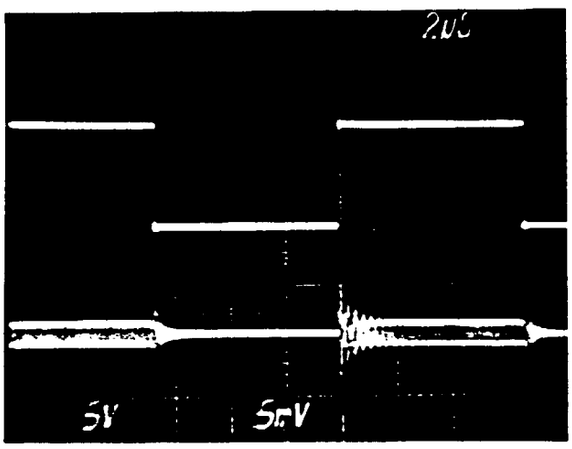

Figure 10: Unbuffered and unfiltered voltage received across a receiver coil at >2 feet distance from an on-chip transmitter.

integrated on chip, without the use of hybrid components which would consume a large volume and require large bonding pads to connect them to the circuit. The most critical element of this design is the transmitter coil. We have developed a fabrication process that will allow us to construct a high quality coil that can function with low losses at ≥20MHz. This process consists of depositing an electroplating base on a wafer, then forming a thick photoresist mold, followed by electroplating a metal such as nickel, gold, copper, etc. using the photoresist mold.

Figure 9 shows a SEM photograph of part of an on-chip electroplated nickel coil to be used for data transmission. It is a 20µm thick, 10 turn rectangular coil with average dimensions of 1.24mm by 7.42mm, a measured inductance of 1.2µH, a series resistance of 90Ω, and a self resonance of >40MHz, all of which are closer than 10% variation from calculated values. The coil has a measured quality factor, $Q=\frac{\omega L}{R}$, of 2.8 at 33MHz, and this could be increased by a factor of 5-10 using other electroplating materials, such as copper or silver. The transmitter operates at a nominal frequency of 33MHz, but can be tuned to a range of between 20MHz and 60MHz. The transmitter has been operated with this coil, and Figure 10 shows a picture of an unbuffered and unfiltered 33MHz AM voltage received with an external coil >2 feet away from the transmitter coil.

CONCLUSIONS

The paper reports the development of a multichannel microstimulator system for FNS. The circuit chip has been fabricated and full device functionality has been shown with an RF telemetric link. This system is the first of its kind providing all of the necessary functions needed for many future wireless instrumentation systems, including voltage regulation, data detection, clock generation, output drive, and active on-chip transmission of data using a single-chip, fully IC compatible fabrication design. This system can be used as a prototype in designing a platform for other microtransducer and microactuator applications.

ACKNOWLEDGMENTS

The authors wish to thank Dr. F. T. Hambrecht and Dr. W. J. Heetderks of the National Institute of Health for their guidance and encouragement. We would also like to thank Dr. Michael Putty and the General Motors Research, Warren, Michigan, for their help in developing the electroplated coil fabrication technology. This work was supported by the Neural Prosthesis Program, NIH, under contract number NIH-NINCDS-N01-NS-4-2319.

REFERENCES

[1] B. Smith, P. H. Peckham, M. W. Keith, D. D. Roscoe, "An Externally Powered, Multichannel, Implantable Stimulator for Versatile Control of Paralyzed Muscle," *IEEE Trans. Biomed. Eng.*, vol. 34, pp. 499-508, July 1987.

[2] B. Ziaie, M. Nardin, J. Von Arx, and K Najafi, "A Single Channel Implantable Microstimulator for Functional Neuromuscular Stimulation (FNS)," *Proceedings, 7th Int. Conf. on Solid-State Sensors and Actuators*, Yokohama, Japan, 450-453, June 1993.

[3] M. Soma, "Reliability of Implantable Electronic Devices: Two Case Studies," *IEEE Trans. Rel.*, vol. R-35, no. 5, pp. 483-7, Dec. 1986.

[4] T. Akin, B. Ziaie, and K. Najafi, "RF Telemetry Powering and Control of Hermetically-Sealed Integrated Sensors and Actuators," *Digest, Solid-State Sensor & Actuator Workshop*, pp. 145-148, Hilton Head, SC, June 1990.

13th International Symposium on Biotelemetry
Williamsburg, VA, April, 1995

AN INDUCTIVELY POWERED MICROSTIMULATOR FOR FUNCTIONAL NEUROMUSCULAR STIMULATION

M. Nardin, B. Ziaie, J. Von Arx, A. Coghlan, M. Dokmeci, and K. Najafi
Center for Integrated Sensors and Circuits
Department of Electrical Engineering and Computer Science
University of Michigan
Ann Arbor, Michigan 48109-2122

ABSTRACT

This paper describes an implantable microstimulator for functional neuromuscular stimulation applications. The microstimulator receives power and data through RF telemetry, and delivers constant current pulses of 10 mA into the muscle tissue through high current Iridium oxide thin-film microelectrodes. A hermetic packaging technique with multiple feedthrough lines has been developed to encapsulate the receiver circuitry and hybrid elements. The overall dimensions of the device are 2x2x10 mm^3.

INTRODUCTION

Functional Neuromuscular Stimulation (FNS) has been widely used to restore function to paralyzed muscles in paraplegic and quadriplegic patients (Smith, 87). A variety of different stimulators have been used to deliver current pulses to dysfunctional muscles. To date, most of these stimulators have been fabricated using long metal wires for stimulating electrodes, hybrid elements for internal circuitry, and large packages. Although these systems have demonstrated the benefits of FNS, it is believed that in order to fully realize these benefits, microstimulators that contain both electrodes and circuitry in one small injectable device are necessary. Over the past several years we have developed a small implantable single channel microstimulator which is powered and controlled through wireless RF telemetry and provides many improvements over existing devices in terms of size and functionality.

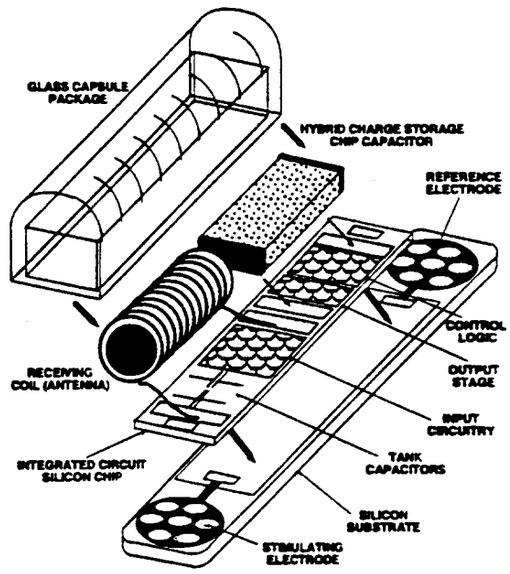

Figure 1: Overall structure of a single channel microstimulator for FNS.

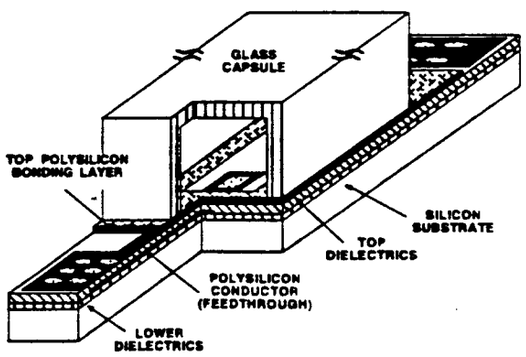

Figure 2: The microstimulator packaging structure.

MICROSTIMULATOR CONSTRUCTION

The overall structure of the single channel microstimulator that has been developed at the University of Michigan is shown in Figure 1. It consists of five individual elements: a micromachined silicon substrate; a silicon IC chip; a hybrid capacitor used for charge storage of the stimulation pulse; a hybrid receiver coil for power and data reception; and a custom machined glass capsule. The silicon substrate contains a reference electrode and a stimulating electrode. The IC chip is used for data reception and microstimulator control and is affixed atop the silicon substrate, while the hybrid capacitor and receiver coil are mounted on the IC chip. A hermetic package is provided for the microstimulator circuitry and hybrid components by electrostatic bonding of the glass capsule to the silicon substrate. The stimulating electrodes are outside of the package and feedthroughs are used to connect the internal electronics to the electrodes. The size of the microstimulator is limited such that it can be injected into the muscle tissue by expulsion from a hypodermic needle. The overall dimensions of the device are 2x2x10 mm^3. Power and data are transmitted to the microstimulator using wireless RF telemetry, and the device is capable of delivering a constant current pulse of 10 mA for durations of up to 200 μsec into loads of ≤800 Ω, and it is able to repeat this stimulation at a rate of up to 40 Hz (Ziaie, 93a). Due to the desired chronic usage of the microstimulator for many applications, the package and electrodes should be capable of operation in vivo for ≥10 years without failure.

PACKAGE DESIGN

As was mentioned in the previous section, the microstimulator receiver circuitry and hybrid elements must be protected from the body fluids for a period of at least 10 years. This requires a hermetic package capable of withstanding harsh body environment throughout the device operating lifetime. Figure 2 shows the packaging technique that was adopted for the encapsulation of the microstimulator. Anodic bonding of a custom made glass capsule to a fine grain polysilicon overlayer was used to protect the receiver circuitry and hybrid elements (Ziaie, 93b; Von Arx, 95). This is a very simple technique that requires heating the glass capsule and the silicon substrate to ~320 °C while keeping the glass at a negative potential of ~2000 V with respect to the silicon substrate. This generates a high electric field at the glass-silicon interface and causes a chemical bond between silicon and glass (Spangler, 87) that is stronger than either of the materials. Figure 3 shows a SEM of a glass capsule bonded to a silicon substrate. The bonding temperature is kept low by using a polysilicon overlayer, reducing any damage to the hybrid elements.

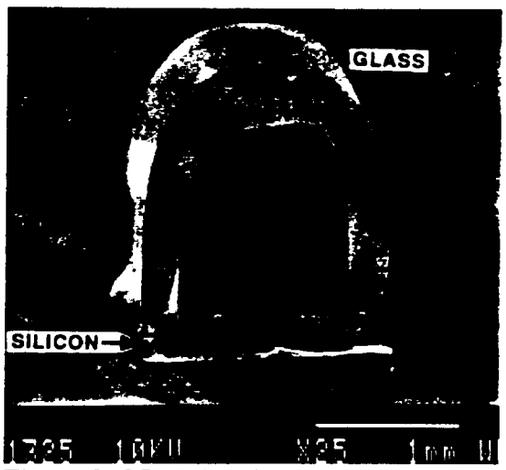

Figure 3: SEM showing a glass capsule bonded to a silicon substrate.

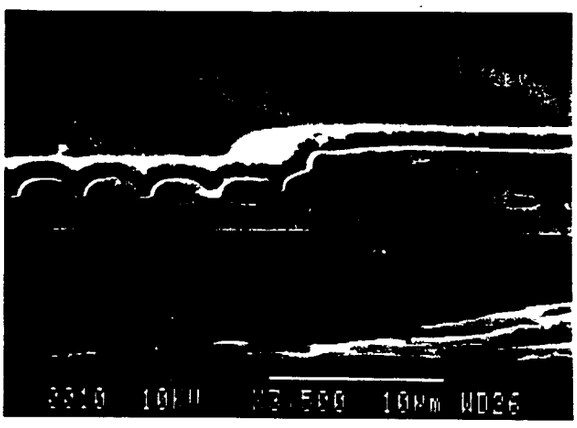

Figure 4: SEM showing the high degree of planarity over the feedthrough lines.

The stimulating electrodes outside the package are connected to the receiver circuitry inside by using a new feedthrough technique (Von Arx, 95). This technique uses closely spaced polysilicon lines (200 lines per mm) that are covered by phosphosilicate glass (PSG) and subsequently reflown at 1200 °C. This produces a planar surface on top of the feedthrough lines as is shown in Figure 4. This planarity is critical for a successful bond since any step over the feedthrough lines prevents a good bond and can cause moisture leakage inside the package. We have also incorporated a dew point sensor inside the package to monitor any moisture condensation during soak tests.

In order to study the package reliability and lifetime, we have started saline soak tests at elevated temperatures (85 and 95 °C). Our goal has been the measurement of activation energy, and accelerating factor for these packages. This will enable us to extrapolate their expected lifetime at body temperature. The initial results are very encouraging and a soak test lifetime of >200 days at 95 °C are currently obtained for these packages (Von Arx, 95), which corresponds to a lifetime of at least ten years at body temperature.

ELECTRODE DESIGN

The microstimulator electrode should be capable of injecting 2 μC of charge in 200 μsec (10 mA) through a small area designated to it (2 mm x 0.5 mm). This is a large amount of charge and conventional electrode materials (e.g., platinum and stainless steel) are unable to inject this amount of charge through such a small area without causing irreversible electrochemical reactions and gas evolution (this is due to their low charge injection capability). Recently, anodically prepared Iridium oxide (IrOx) film has attracted much attention as a high charge injection capability material suitable for small stimulating electrodes (Robblee, 83). IrOx was chosen for the microstimulator electrode material due to its large charge injection capability.

Following this choice, simple planar electrodes were fabricated and subjected to 10 mA current pulses. These electrodes showed high current density around the perimeter (this is called the edge effect) (Rubenstein, 87) which caused film delamination and eventual failure as is shown in Figure 5. In order to overcome this problem a new electrode was designed that maintains the same total area while having a larger perimeter (Ziaie, 91). This was achieved by dividing the total area into many small sites connected in parallel each one carrying a portion of the total current. A picture of this new electrode,

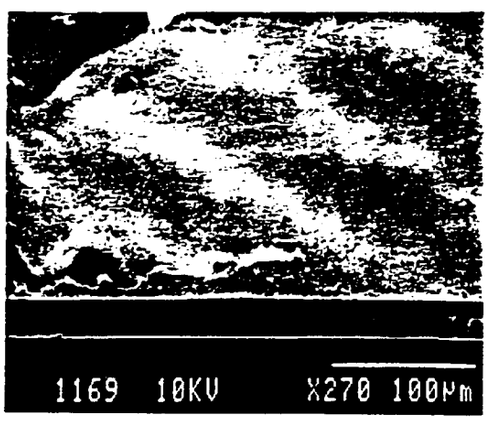

Figure 5: High current density damage around the perimeter of a planar electrode.

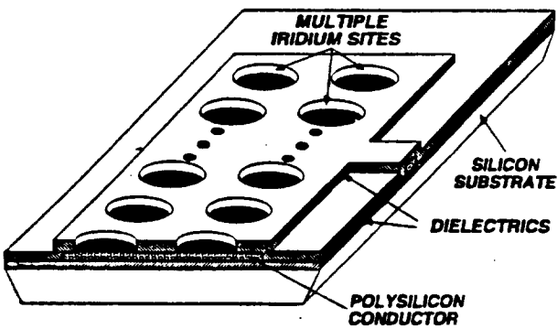

Figure 6: The waffle electrode structure.

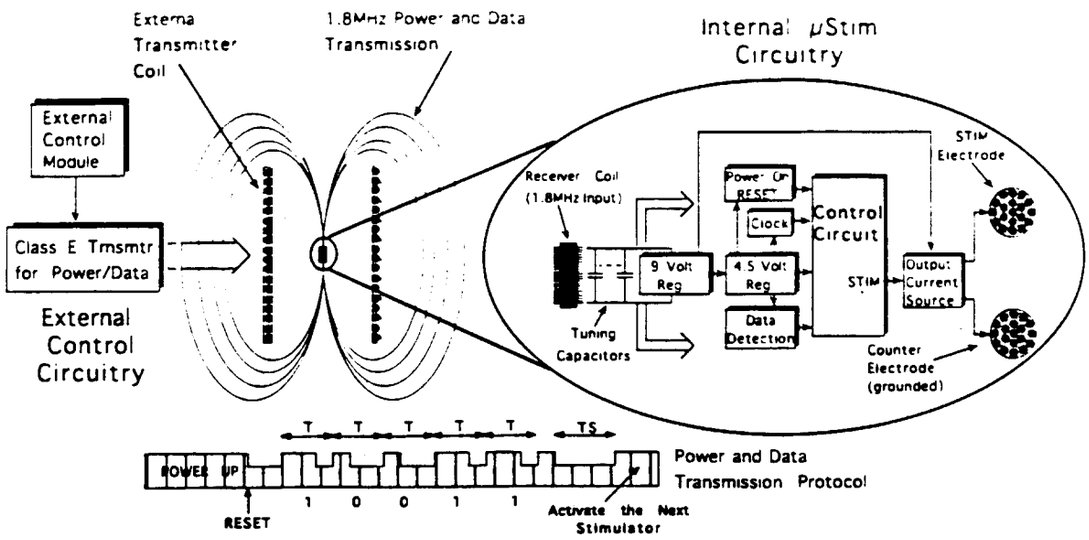

Figure 7: Overall system block diagram and data transmission protocol for a 5 bit addressable single channel microstimulator.

called the waffle electrode due to its appearance, is shown in Figure 6. The increased perimeter to area ratio produced by this design effectively reduces the current density around the perimeter of the electrode (Ziaie, 91). These electrodes were subsequently tested with 10 mA current pulses in saline and were able to withstand more than 2 billion current pulses without any sign of degradation.

MICROSTIMULATOR CIRCUITRY

Figure 7 shows the overall system block diagram and data transmission protocol for the microstimulator. The device receives power and data through RF telemetry, using amplitude modulation of a 2 MHz carrier. After power-on, the carrier amplitude is momentarily turned low to reset all of the circuit blocks on the receiver chip and is then modulated to transmit a 5-bit address to up to 32 microstimulators located within the volume of the transmitter coil. After a specific microstimulator is selected, the carrier signal is turned high and then back low again. It is maintained at this low level for a period between 1-200 μs. The selected microstimulator will then deliver a constant current pulse of 10 mA into the tissue through the stimulating electrode pair for the period of time that the carrier is low. Finally, the carrier is turned back high again, which will indicate the end of the stimulation period to the selected microstimulator, thus allowing it to charge its capacitor back up to the on-chip voltage supply.

The receiver circuitry for the microstimulator contains five main circuit blocks: 4.5 V and 9 V voltage regulators, an envelope detector for data reception, clock recovery circuitry, a control circuit, and an output pulse delivery circuit. Some of these circuit blocks have conflicting requirements. The voltage regulators, envelope detector, and clock circuitry must all have protection from the high voltage input signal and consume relatively low power, while the control circuit should be a low voltage/power CMOS design, and the output circuit must be able to deliver relatively high level constant current pulses. In order to satisfy these requirements for the microstimulator circuitry, we have developed a combined bipolar-CMOS circuit technology in our facility (Ziaie, 91). A picture of the fabricated circuit chip is shown in Figure 8. This receiver circuitry has been tested and verified to be fully functional. Figure 9 shows results from a complete microstimulator

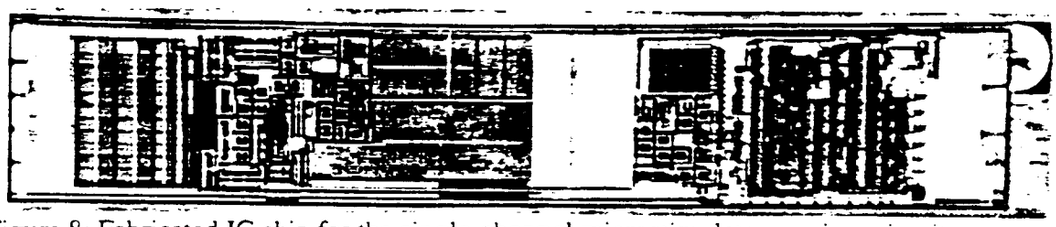

Figure 8: Fabricated IC chip for the single channel microstimulator receiver circuitry.

Operating Range for Received Input Voltage	Working μStim for **10V-21V Range** for the Peak Received Voltage
Voltage Regulation Circuitry	9V Regulator has **<0.5V Ripple** 4.5V Regulator has **<0.2V Ripple**
Output Stimulation Pulse Circuitry	Provides Constant Current Pulses of **10mA** Across Variable Loads ≤ 800 Ω for Durations of **up to 200μsec**
Power Consumption	Consumes ≤3mA Current at 20V Peak Sinusoidal Input Voltage (**≤60mW**)

Table 1: Overall results from operation of a single channel microstimulator.

circuit: the modulated carrier received through RF telemetry, the demodulated data, and the stimulation current pulse. A summary of these test results is shown in Table 1.

CONCLUSIONS

We have developed a telemetrically controlled microstimulator for FNS applications. A hermetic packaging technique with multiple feedthroughs was used to enclose the receiver circuitry and hybrid elements. A high current capability IrOx thin-film stimulating microelectrode was developed to deliver large amounts of charge to the muscle tissue. The microstimulator is controlled by an IC silicon chip that was constructed using a custom bipolar-CMOS fabrication technology. The overall microstimulator dimensions are $2x2x10mm^3$ and a photograph of an assembled microstimulator on a penny is shown in Figure 10. Due to its small size and wireless nature, it might be ideal in chronic implant situations where FNS had previously been unsuitable.

ACKNOWLEDGMENTS

The authors wish to thank Dr. F. T. Hambrecht and Dr. W. J. Heetderks of the National Institute of Health for their guidance and encouragement. We would also like to thank Dr. Michael Putty and the General Motors Research, Warren, Michigan, for their assistance in fabrication of the microstimulator packaging, Dr. T. Akin for helping in fabrication of the microstimulator circuitry, and Dr. Y. Gianchandani for the design of the control circuitry. This work was supported by the Neural Prosthesis Program, NIH, under contracts numbered NIH-NINCDS-N01-NS-8-2312 and NIH-NINCDS-N01-NS-4-2319.

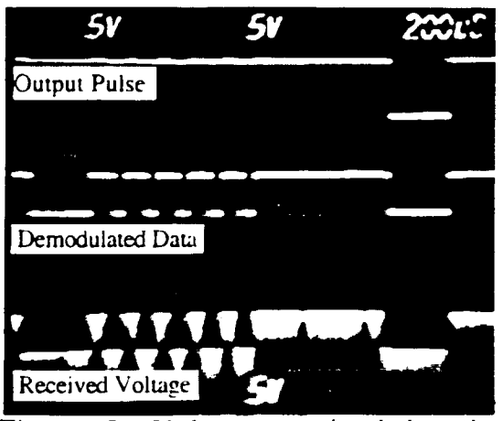

Figure 9: Voltage received by the microstimulator, demodulated data, and output stimulation pulse across an 820Ω load.

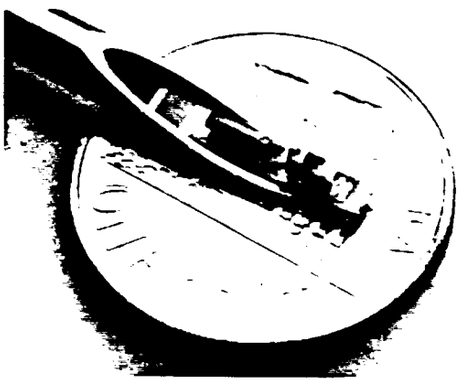

Figure 10: Photograph showing an assembled microstimulator on a penny. The device measurements are 2x2x10 mm^3.

REFERENCES

Robblee, L. S., J. L. Lefko, and S. B. Brummer, "Activated Iridium: An Electrode Suitable for Reversible Charge Injection in Saline Solution," *J. Electrochem. Soc.*, Vol. 130, pp. 731-733, 1983.

Rubenstein, J. T., F. A. Spelman, M. Soma, and M. F. Susserman, "Current Density Profile of Surface Mounted Recessed Electrodes for Neural Prosthesis," *IEEE Trans. Biomed. Eng.*, vol. 34, pp. 864-875, Nov. 1987.

Smith, B., P. H. Peckham, M. W. Keith, and D. D. Roscoe, "An Externally Powered, Multichannel, Implantable Stimulator for Versatile Control of Paralyzed Muscle," *IEEE Trans. Biomed. Eng.*, vol. 34, pp. 499-508, July 1987.

Spangler, L. J., and K. D. Wise, "A Technology for High-Performance Single-Crystal Silicon-on-Insulator Transistors," *IEEE Electron Device Letters.*, vol. 8, pp. 137-139, April 1987.

Von Arx, J., B. Ziaie, M. Dokmeci, and K. Najafi, "Hermeticity Testing of Glass-Silicon Packages with On-Chip Feedthroughs," *Proceedings, 8th Int. Conf. on Solid-State Sensors and Actuators,* Stockholm, Sweden, June 1995.

Ziaie, B,Y. Gianchandani, and K Najafi, "A High-Current IrOx thin-Film Neuromuscular Microstimulator," *Proceedings, 6th Int. Conf. on Solid-State Sensors and Actuators,* pp. 124-127, San Francisco, June 1991.

Ziaie, B, M. Nardin, J. Von Arx, and K Najafi, "A Single Channel Implantable Microstimulator for Functional Neuromuscular Stimulation (FNS)," *Proceedings, 7th Int. Conf. on Solid-State Sensors and Actuators,* pp. 450-453, Yokohama, Japan, June 1993(a).

Ziaie, B, J. Von Arx, M. Nardin, and K Najafi, "A Hermetic Packaging Technique with Multiple Feedthroughs for Integrated Sensors and Actuators," *Proceedings, 7th Int. Conf. on Solid-State Sensors and Actuators,* pp. 266-269, Yokohama, Japan, June 1993(b).